# Supporting information

## *Access to long-lived room temperature phosphorescence through auration of 2,1,3-benzothiadiazole*

Mauricio Posada Urrutia,†[a] Nidhi Kaul,†[b] Tobias Kaper,[a] Dustin Hurrell,[c] Linus Chiang,[c] Jordann A.L. Wells,[b] Andreas Orthaber,[b] Leif Hammarström, [b] Lukasz T. Pilarski,[a] and Christine Dyrager *[a]

†These authors contribute equally.

[a.] Department of Chemistry-BMC, Uppsala University, Box 576, 751 23 Uppsala, Sweden.
[b.] Department of Chemistry-Ångström, Uppsala University, Box 523, 751 20 Uppsala, Sweden.
[c.] Department of Chemistry, University of the Fraser Valley, V2S7M8, Abbotsford, BC, Canada.

## Table of Contents

## I. General information

All reagents were purchased from Sigma-Aldrich (Merck) or Fluorochem and used without further purification. Solvents used for synthesis were obtained from VWR Chemicals and used without further purification unless otherwise specified. 1,4-Dioxane was dried over activated 4Å molecular sieves. Solvents for photophysical measurements were used without further purification: dichloromethane (Uvasol, Merck/Supelco); anhydrous 2-methyltetrahydrofuran (2-Me-THF) of ≥99% purity (Sigma-Aldrich). These solvents were degassed in a Schlenk flask sealed with greased joints by 4 cycles of freeze-pump-thaw before the photophysical measurements. Thin-layer chromatography (TLC) was carried out using aluminum plates coated with silica gel ($60F_{254}$, Merck) and visualized through exposure to UV light ($\lambda$ = 254 nm and/or 365 nm). NMR spectra were recorded at 298 K on an Agilent MR400-DD2 (400 MHz) spectrometer with a OneNMR probe at 400 MHz ($^{1}$H), 101 MHz ($^{13}$C), 162 MHz ($^{31}$P), or 128.3 MHz ($^{11}$B). Chemical shifts ($\delta$) are reported in ppm using the residual solvent peak in $CDCl_3$ ($\delta_H$ = 7.26 and $\delta_C$ = 77.2 ppm) or $C_6D_6$ ($\delta_H$ = 7.16 and $\delta_C$ = 128.1 ppm) as internal reference. $^{31}$P chemical shifts were referenced via the lock signal to $H_3PO_4$. $^{11}$B chemical shifts were referenced via the lock signal to $BF_3{\bullet}Et_2O$. Coupling constants (*J*) are given in Hz and the apparent resonance multiplicity is reported as s (singlet), d (doublet), t (triplet), q (quartet), or m (multiplet). Assignment of the $^{1}$H and $^{13}$C spectra were done with the help of $^{1}$H-$^{13}$C HMBC and $^{1}$H-$^{13}$C HSQC experiments. High-resolution mass spectrometry (HRMS) data, (ES-ToF), was determined at the Division of Mass Spectrometry, Department of Chemistry, Imperial College London, UK.

**X-ray crystallography**

Single crystals of complexes **3a**-**e** were obtained by slow diffusion of pentane into concentrated $CH_2Cl_2$ solutions. Measurements were performed using graphite-monochromatized Mo Kα radiation at 170 K using a Bruker D8 APEX-II equipped with a CCD camera. The structure was solved by direct methods (SHELXS-2014) and refined by full-matrix least-squares techniques against F2 (SHELXL-2018). The non-hydrogen atoms were refined with anisotropic displacement parameters. The H atoms of the $CH_2$/CH groups were refined with common isotropic displacement parameters for the H atoms of the same group and idealized geometry. The H atoms of the methyl groups were refined with common isotropic displacement parameters for the H atoms of the same group and idealized staggered geometry. CCDC 2026788 and 2125287-2125290 contain the supplementary crystallographic data for this paper. The data can be obtained free of charge from The Cambridge Crystallographic Data Centre via www.ccdc.cam.ac.uk/structures.

**Steady-state absorption and emission measurements**

All the complexes were recrystallized twice before any measurement. This was done by slow diffusion of pentane into concentrated $CH_2Cl_2$ solutions.

UV/Vis absorption spectra were acquired on a UV-1650PC Shimadzu instrument (measurements in $CH_2Cl_2$) or on a Varian Cary 5000 spectrophotometer (measurements in 2-Me-THF) at room temperature using quartz cuvettes (10 mm path length). Absorption maxima ($\lambda_{max}$) are reported in nm and the molar extinction coefficient ($\varepsilon$) in $M^{-1}\,cm^{-1}$. For each compound three data points with known different concentrations were acquired and the measured absorbances (≤1) were plotted against the concentrations. The molar extinction coefficients were then determined according to the Lambert-Beer law as the slope of the linear fit.

Steady-state emission and excitation spectra at room temperature were recorded on a FS5 Spectrofluorometer (Edinburgh Instruments) equipped with a SC-20 (thermostatic) sample holder, in a standardized right-angle geometry configuration. For the measurements, excitation and emission slit widths corresponding to spectral resolutions of 4 nm and 1 nm were used, and the integration time was 0.5 s. For the excitation spectrum shown for monitoring at 620 nm, however, the excitation width was lowered to 2 nm since a *ca.* 150 µM stock solution was used; the integration time was 0.2 s. All data were automatically corrected for detector response using the supplied correction file from the manufacturer by the data collection software, Fluoracle, on the attached computer.

Emission data collected at 298K were obtained from measurements using freeze-pump thaw degassed solvents. Samples were prepared inside an Argon-filled glovebox and the measurements were carried out in Hellma sealable cells (article number: 117100F-10-40) that had their threads lined with PTFE tape before being sealed. The initial solutions of **3a-e** were made by preparing a volumetric solution of the pre-weighed compound and then further diluting it by volume so that all measured solutions were of 15 µM concentration. Phosphorescence quantum yields were determined by carrying out relative actinometry, *i.e.,* by comparison with the integrated emission intensity of a standard phosphor with known quantum yield, measured under identical conditions. The phosphor used was $[Ru(bpy)_3]^{2+}$ with a reported quantum yield of 0.018 in aerated acetonitrile,[1] and a suitable emission in the red, centred at 620 nm, very similar to the gold complexes. The quantum yields of the samples could thus be determined using the following equation:

$$\phi_x = \phi_s \times \frac{I_x}{I_s} \times \frac{A_s}{A_x} \times \frac{\eta_x}{\eta_s}$$

where $\phi_x$ is the quantum yield of the sample, $\phi_s$ is the known quantum yield of the standard, $I_x$ and $I_s$ are the integrated emission intensities of the sample and standard, respectively, and $\eta_x$ and $\eta_s$ are the respective refractive indices of the sample and standard solutions, often approximated as those of the solvents for dilution solutions (which is the case here). Finally, $A_x$ and $A_s$ are the absorbances of the sample and standard, typically kept as close as possible at the given excitation wavelength (355 nm in this case). For these measurements, extra care was taken and a calibration curve for the standard fluorophore, $[Ru(bpy)_3][PF_6]_2$, was made (Figure S1) so that the integrated emission intensity at any given absorbance <0.1 could be estimated for the standard and compared with the sample. The results are shown in Table 2 in the paper.

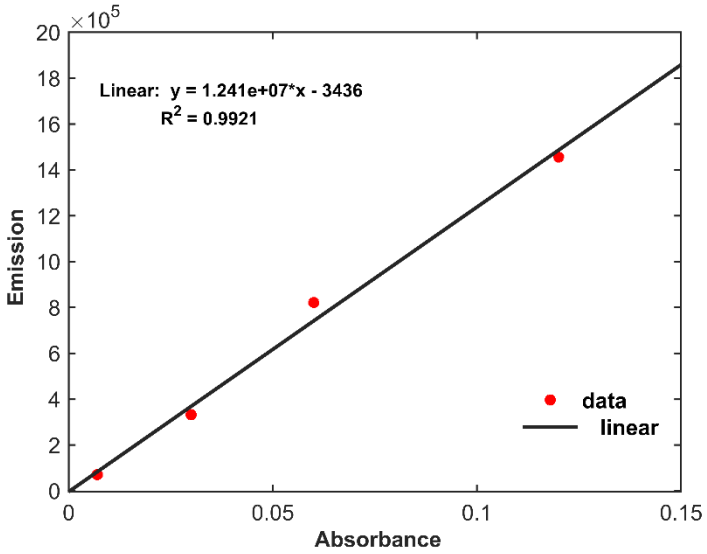


**Figure S1.** Calibration curve for $[Ru(bpy)_3][PF_6]_2$ for the determination of the phosphorescence quantum yield of the gold complexes.

Steady-state emission spectra at 77K were collected using a Horiba Jobin Yvon Fluorolog-3 by employing a cold-finger setup, with liquid nitrogen as coolant. Excitation and emission slit widths corresponding to spectral resolutions of 2 nm and 1 nm were used, and the integration time was 0.1 s. All data were corrected for detector response and fluctuation in excitation intensity.

**Time-resolved spectroscopic measurements**

*Time-correlated single photon counting (TCSPC).* TCSPC measurements were carried out to determine the fluorescence lifetimes of the gold complexes. The decay traces were recorded using an FS5 fluorometer, with an SC-20 sample holder, as described above. The excitation source was changed to a pulsed sub-ns excitation source, EPLED340. The typical pulse-width was 810 ps, with an average power of 1 µW at 10 MHz. The detector employed was an air-cooled and stabilized HS-PMT-920. The monitoring wavelength was 425 nm, and a bandpass corresponding

to a spectral width of 10 nm was used. The measurement range was 200 ns and 4096 channels were chosen for the multi-channel analyzer on the collection software, Fluoracle. The so-obtained decays were fit using the curve fitting tool in MATLAB R2020b and were amenable to a monoexponential fit.

*Time-resolved emission measurements (TRE).* Nanonsecond time-resolved emission measurements were made to accurately determine the phosphorescence lifetimes of the gold complexes. A Q-switched Nd:YAG laser (Model NT342B, EKSPLA; FWHM = *8* ns), was used as the excitation source, whose fundamental emission at 1064 nm was frequency tripled to produce 355 nm light. The output was then attenuated using a series of neutral density filters and used to excite the sample. The repetition rate was 10 Hz, and the pump energy was maintained at <0.8 mJ/pulse (±10%) to minimize photodegradation; absorption spectra were measured before and after measurements to confirm sample integrity, and typical differences were less than 5%. The setup utilized a right-angle detection geometry. The LP920 detection system (Edinburgh Instruments) equipped with a photomultiplier tube was used to record the kinetic data, which was collected using the L900 software (which controlled the Tektronix digital oscilloscope) on the connected computer. The decay traces were recorded with a consistent resolution of 5 nm, and a 435 nm cut-off filter was used to minimize contamination from scattered laser light. Every measurement was averaged over 8 shots. The so-obtained decays were binned every ten points, and then fit using the curve fitting tool in MATLAB R2020b and were amenable to a monoexponential fit model.

**Computational details**

Geometry optimizations without symmetry constraints were carried out with the Gaussian 16 software (revision A.03),[2] using the hybrid density functional PBE0,[3] with a polarized continuum model (PCM) for $CH_2Cl_2$ (dielectric ε = 8.94).[4] The 6-31G*[5-7] basis set was used for all atoms except Au, which was described by the Stuttgart relativistic pseudopotential and accompanying basis set ECP60MWB.[8, 9] This combination of functional and basis set has been previously used to investigate structurally similar Au complexes.[10, 11] Frequency calculations were performed at the same level of theory to ensure that the optimized structures were located at a potential energy surface minimum by the absence of imaginary frequencies. Stability calculations were also performed for all optimized structures to ensure that all wavefunctions were stable. Vertical excitation energies to singlet and triplet excited states were calculated using time-dependent density functional theory (TD-DFT) at the same level of theory with a PCM for $CH_2Cl_2$.

**Electrochemical analysis**

Cyclic voltammetry (CV) was performed on an Epsilon potentiometer equipped with an Ag wire reference electrode, a platinum wire counter electrode and a glassy carbon working electrode. All CV experiments were performed on THF solutions comprising of 2.0 mM of analyte (**3a**-**e**) and $^{n}Bu_4NPF_6$ (0.1 M) as supporting electrolyte. Ferrocene was used as an internal standard.[12]

## II. Synthesis

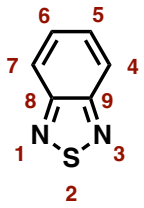


**Figure S2.** Structure and numbering of 2,1,3-benzothiadiazole (BTD).
$^{1}$H NMR (400 MHz, $C_6D_6$) δ 7.77 – 7.61 (m, 2H, H4/7), 7.00 – 6.82 (m, 2H, H5/6). $^{13}$C NMR (101 MHz, $C_6D_6$) δ 155.2 (C8/9), 129.0 (C4/7), 121.7 (C5/6).

**Benzo[c][1,2,5]thiadiazol-4-ylboronic acid (2).**

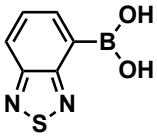


A 50 mL oven-dried two-neck round-bottom flask was loaded with a magnetic stir-bar, 4-bromo-2,1,3-benzothiadiazole (2.00 g, 9.30 mmol), KOAc (2.74 g, 27.9 mmol) and $B_2(pin)_2$ (2.83 g, 11.16 mmol). The flask was flushed with Ar and then fitted with a reflux condenser attached to a constant Ar flow. Dry 1,4-dioxane (30 mL) was added and the suspension was degassed by bubbling Ar through the solution for 30 min. $PdCl_2$(dppf) (0.408 g, 0.56 mmol, 6.0 mol%) was added in a single portion. The reaction mixture was stirred at reflux for 90 min and then to cooled to rt. The crude mixture was filtered through a layer of Celite. The reaction flask was rinsed with $Et_2O$ (120 mL), which was used to further flush the Celite plug. The organic layer was washed with brine (2 × 80 mL) and $H_2O$ (80 mL), dried ($MgSO_4$), filtered and concentrated under reduced pressure until 30 mL of solvent remained. The solution was heated to reflux and, under strong stirring, diethanolamine (1.17 g, 11.16 mmol) was added. The reaction was stirred for 30 min, at which point a dark brown oil had formed. The solution was transferred to a separatory funnel and the reaction flask was rinsed out with $H_2O$ (60 mL) until no viscous residue remained in the flask. The aqueous phase was transferred to the separatory funnel and the layers were separated. The organic layer extracted further with $H_2O$ (2 × 60 mL). The combined aqueous layers were acidified with $HCl_{(aq)}$ (4M) and stirred for 5 min. The resulting precipitate was filtered off and thoroughly rinsed with $H_2O$. The residue was dissolved in MeOH and the solution was dried under reduced pressure to afford compound **2** as a light-pink solid (1.03 g, 62 %). $^{1}$H NMR (400 MHz, $CDCl_3$) δ 8.23 (dd, *J* = 6.5, 1.0 Hz, 1H), 8.13 (dd, *J* = 8.8, 1.0 Hz, 1H), 7.69 (dd, *J* = 8.8, 6.5 Hz, 1H), 6.42 (s, 2H); $^{13}$C NMR (101 MHz, $CDCl_3$) δ 158.5, 154.3, 138.0, 129.7, 124.2 (The *C*–B signal was not observed due to quadrupolar relaxation); $^{11}$B NMR (128 MHz, $CDCl_3$) δ 28.7. HR-MS: (ESI-TOF) calcd for $[C_6H_5BN_2O_2S + H]^+$ = 181.0238; found 181.0237.

**BTD–Au(I)–$PPh_3$ (3a)**

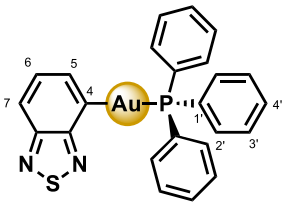

Compound **2** (21.6 mg, 0.12 mmol), chloro(triphenylphosphine)gold(I) (56.4 mg, 0.11 mmol) and KOH (14.8 mg, 0.26 mmol) were stirred in EtOH (1 mL) for 24 hours. The solution was centrifuged, the supernatant was removed, and the solid residue washed with EtOH (3 × 1 mL). Compound **3a** was obtained as a colourless solid (63 mg, 88 %). $^1$H NMR (400 MHz, $C_6D_6$) δ 8.08 (ddd, $J_{H\text{-}H}$ = 6.33, $J_{H\text{-}P}$ = 6.27, $J_{H\text{-}H}$ = 1.2 Hz, 1H, H5), 7.90 (ddd, $J_{H\text{-}H}$ = 8.7, $J_{H\text{-}H}$ = 1.2, $J_{H\text{-}P}$ = 0.7 Hz, 1H, H7), 7.59-7.48 (m, 6H, H2'), 7.38 (ddd, $J_{H\text{-}H}$ = 8.68, $J_{H\text{-}H}$ = 6.33, $J_{H\text{-}P}$ = 1.1 Hz, 1H, H6), 6.97 (m, 9H, H3' and H4'); $^{13}$C NMR (101 MHz, $C_6D_6$) δ 170.1 (d, $J_{C\text{-}P}$ = 116.5 Hz, C4), 165.0 (C9), 155.5 (d, $J_{C\text{-}P}$ = 4.1 Hz, C8), 139.2 (C5), 134.7 (d, $J_{C\text{-}P}$ = 13.8 Hz, C2'), 131.7 (C4'), 131.2 (d, $J_{C\text{-}P}$ = 2.4 Hz, C1'), 129.5 (d, $J_{C\text{-}P}$ = 6.7 Hz, C6), 129.3 (d, $J_{H\text{-}P}$ = 10.8 Hz, C3'), 118.5(C7); $^{31}$P NMR (162 MHz, $C_6D_6$) δ 42.8. HR-MS: (ESI-TOF) calcd. for $[C_{24}H_{18}N_2PSAu + H]^+$ = 595.0672; found 595.0667.

**BTD–Au(I)–P$^t$Bu$_3$ (3b)**

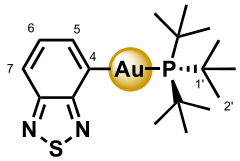

Compound **2** (22 mg, 0.12 mmol), chloro(tri-*tert*-butylphosphine)gold(I) (43 mg, 0.10 mmol) and KOH (14 mg, 0.25 mmol) were stirred in EtOH (1mL) for 24 hours. The solution was centrifuged, the supernatant was carefully removed, and the solid residue washed with EtOH (3 × 1 mL). Compound **3b** was obtained as a colourless solid (51 mg, 78 %). $^1$H NMR (400 MHz, $C_6D_6$) δ 8.03 (ddd, $J_{H\text{-}H}$ = 6.3, $J_{H\text{-}P}$ = 5.4, $J_{H\text{-}H}$ = 1.2 Hz, 1H, H5), 7.88 (ddd, $J_{H\text{-}H}$ = 8.7, $J_{H\text{-}H}$ = 1.2 Hz, $J_{H\text{-}P}$ = 1.0 Hz, 1H, H7), 7.37 (ddd, $J_{H\text{-}H}$ = 8.7, $J_{H\text{-}H}$ = 6.3, $J_{H\text{-}P}$ = 1.2 Hz, 1H, H6), 1.26 (d, $J_{H\text{-}P}$ = 12.8 Hz, 27H, H2'); $^{13}$C NMR (126 MHz, $C_6D_6$) δ 173.2 (d, $J_{C\text{-}P}$ = 106.4 Hz, C4), 165.3 (C9), 155.6 (d, $J_{C\text{-}P}$ = 4.1 Hz, C8), 138.7 (C5), 129.5 (d, $J_{C\text{-}P}$ = 6.2 Hz, C6), 118.0 (d, $J_{C\text{-}P}$ = 1.0, C7), 38.8 (d, $J_{C\text{-}P}$ = 14.2 Hz, C1'), 32.3 (d, $J_{C\text{-}P}$ = 4.9 Hz, C2'); $^{31}$P NMR (162 MHz, $C_6D_6$) δ 91.5. HR-MS: (ESI-TOF) calcd. for $[C_{18}H_{30}N_2PSAu + H]^+$ = 535.1611; found 535.1620.

**BTD–Au(I)–$PCy_3$ (3c)**

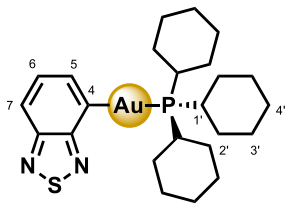

Compound **2** (22 mg, 0.12 mmol), chloro(tricyclohexylphosphine)gold(I) (51 mg, 0.10 mmol) and KOH (14 mg, 0.25 mmol) were stirred in EtOH (1mL) for 24 hours. The solution was centrifuged, the supernatant was carefully removed, and the solid residue washed with EtOH (3 × 1 mL). Compound **3c** was obtained as a colourless solid (56 mg, 92 %). $^1$H NMR (400 MHz, $C_6D_6$) δ 8.09 (ddd, $J_{H\text{-}H}$ = 6.3, $J_{H\text{-}P}$ = 6.0, $J_{H\text{-}H}$ = 1.2 Hz, 1H, H5), 7.87 (ddd, $J_{H\text{-}H}$ = 8.7, $J_{H\text{-}H}$ = 1.2, $J_{H\text{-}P}$ = 1.0 Hz, 1H, H7), 7.37 (ddd, $J_{H\text{-}H}$ = 8.7, $J_{H\text{-}H}$ = 6.3, $J_{H\text{-}P}$ = 1.2 Hz, 1H, H6), 1.98-1.89 (m, 6H), 1.89-1.80 (m, 3H, H1'), 1.69-1.57 (m, 6H), 1.55-1.35 (m, 9H), 1.05 (m, 9H)

$^{13}$C NMR (101 MHz, $C_6D_6$) δ 174.3 (d, $J_{C\text{-}P}$ = 110.0 Hz, C4), 165.3 (C9), 155.7 (d, $J_{C\text{-}P}$ = 4.2 Hz, C8), 138.7 (C5), 129.6 (C6), 118.1 (d, $J_{C\text{-}P}$ = 1.3 Hz, C7), 33.6 (d, $J_{C\text{-}P}$ = 24.4 Hz, C1'), 30.9 (d, $J_{C\text{-}P}$ = 1.4 Hz), 27.4 (d, $J_{C\text{-}P}$ = 11.4 Hz), 26.3 (d, $J_{C\text{-}P}$ = 1.4 Hz); $^{31}$P NMR (162 MHz, $C_6D_6$) δ 56.5 (s). HR-MS: (ESI-TOF) calcd. for $[C_{24}H_{36}N_2PSAu + H]^+$ = 613.2081; found 613.2065

**BTD–Au(I)–IPr (3d)**

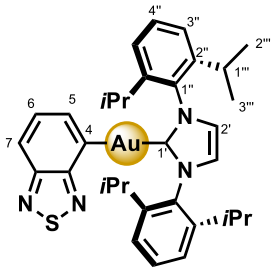


Compound **2** (22 mg, 0.120 mmol), chloro[1,3-bis(2,6-diisopropylphenyl)imidazol-2-ylidene]gold(I) (61 mg, 0.10 mmol) and KOH (14 mg, 0.25 mmol) were stirred in EtOH (1 mL) for 24 hours. The solution was centrifuged, the supernatant was carefully removed, and the solid residue washed with EtOH (3 × 1 mL). Compound **3d** was obtained as a colourless solid (64 mg, 88 %). $^1$H NMR (400 MHz, $C_6D_6$) δ 7.61 (dd, $J$ = 8.7, 1.2 Hz, 1H, H7), 7.54 (dd, $J$ = 6.3, 1.2 Hz, 1H, H5), 7.21 (dd, $J$ = 8.4, 7.1 Hz, 2H, H4''), 7.09 (d, $J$ = 7.9 Hz, 4H, H3''), 7.08 (dd, $J$ = 8.7, 6.3 Hz, 1H, H6), 6.36 (s, 2H, H2'), 2.74 (dq, $J$ = 6.9 Hz, 6.8 Hz, 4H, H1'''), 1.59 (d, $J$ = 6.8 Hz, 12H, H2''' or H3'''), 1.14 (d, $J$ = 6.9 Hz, 12H, H2''' or H3'''). $^{13}$C NMR (101 MHz, $C_6D_6$) δ 196.7(C1'), 166.9 (C4), 165.6 (C9), 155.1 (C8), 146.0 (C2''), 139.2 (C5), 135.0 (C1''), 130.6 (C4''), 129.0 (C6), 124.2 (C3''), 122.7 (C2'), 116.9 (C7), 29.2 (C1'''), 24.9 (C2''' or C3'''), 24.0 (C2''' or C3'''). HR-MS: (ESI-TOF) calcd. for $[C_{33}H_{39}N_4SAu + H]^+$ = 721.2639; found 721.2637

**BTD–Au(I)–IMes (3e)**

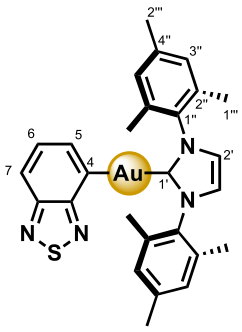


Compound **2** (22 mg, 0.12 mmol), chloro[1,3-bis(2,4,6-trimethylphenyl)imidazol-2-ylidene]gold(I) (54 mg, 0.10 mmol) and KOH (14 mg, 0.25 mmol) were stirred in EtOH (1mL) for 24 hours. The solution was centrifuged, the supernatant was carefully removed, and the solid residue washed with EtOH (3 × 1 mL). Compound **3e** was obtained as a colourless solid (54 mg, 84%). $^1$H NMR (400 MHz, $C_6D_6$) δ 7.62 (dd, $J$ = 6.4, 1.2 Hz, 1H, H5), 7.58 (dd, $J$ = 8.7, 1.2 Hz, 1H, H7), 7.03 (dd, $J$ = 8.7, 6.4 Hz, 1H, H6), 6.72 (s, 4H, H3''), 6.09 (s, 2H, H2'), 2.14 (s, 12H, H1'''), 2.03 (s, 6H, H2'''); $^{13}$C NMR (101 MHz, $C_6D_6$) δ 195.0 (C1'), 167.2 (C8), 166.0 (C9), 155.2 (c4), 139.4 (C2''), 139.2 (C5), 135.7 (C1''), 135.0 (C2''), 129.6 (C3''), 129.2 (C6), 121.7 (C3'), 116.8 (C7) , 21.1 (C2'''), 18.1 (C1'''). HR-MS: (ESI-TOF) calcd. for $[C_{27}H_{27}N_4SAu + H]^+$ = 637.1700; found 637.1689

**Additional information:** The complexes **3a**-**e** have sparing solubility in acetonitrile, good solubility in benzene, THF and 2-Me-THF and, high solubility in $CH_2Cl_2$ and $CHCl_3$. Solutions of **3a**-**e** are stable indefinitely in the dark at low temperature.

## III. Photophysical data

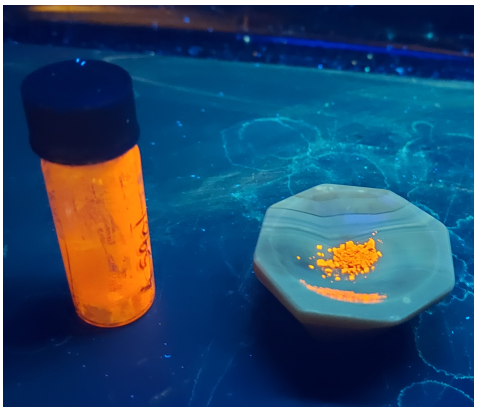

**Figure S3.** Solid state emission of compound **3d** ($\lambda_{ex}$ = 254 nm).

**Table S1.** UV-Vis absorption values for **3a**-**e** in degassed $CH_2Cl_2$ (freeze-pump thaw cycling).

| Compound | $\lambda_{abs}$ (nm) |
|---|---|
| **3a** | 306, 314, 351 |
| **3b** | 305, 312, 348 |
| **3c** | 306, 312, 348 |
| **3d** | 306, 313, 351 |
| **3e** | 306, 313, 353 |

**Table S2**. Absorption and emission data for compound **3d** in solvents of different polarity.

| Solvent | $\lambda_{Abs}$ (nm) | Wavenumber ($cm^{-1}$) | $\lambda_{Em}$ (nm) | Wavenumber ($cm^{-1}$) |
|---|---|---|---|---|
| Hexane | 352 | 28409 | 432 | 23148 |
| Toluene | 354 | 28249 | 444 | 22523 |
| $CH_2Cl_2$ | 356 | 28090 | 469 | 21322 |
| 2-Me-THF | 354 | 28249 | 461 | 21692 |
| Acetonitrile | 353 | 28329 | 476 | 21008 |
| MeOH | 356 | 28090 | 477 | 20964 |

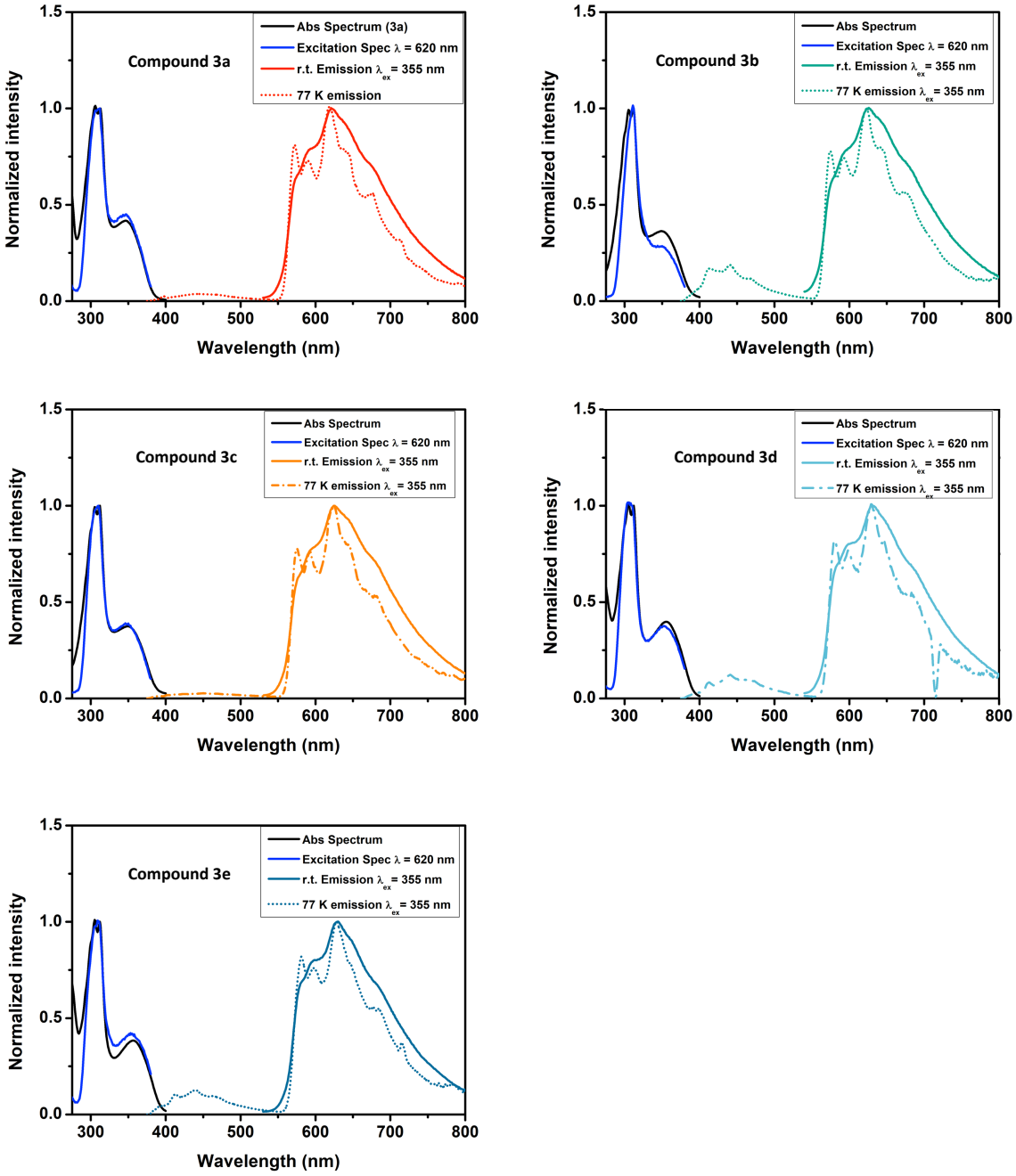


**Figure S4.** Spectroscopic properties of **3a-3e** 2-Me-THF (conc. 15 µM): Absorption spectra at room temperature (under air atmosphere); Excitation spectra at room temperature in degassed solution (monitored at 620 nm); Emission at room temperature in degassed solution recorded at 540-800nm, $\lambda_{ex}$ = 355 nm; Emission at 77K under air atmosphere, $\lambda_{ex}$ = 355 nm.

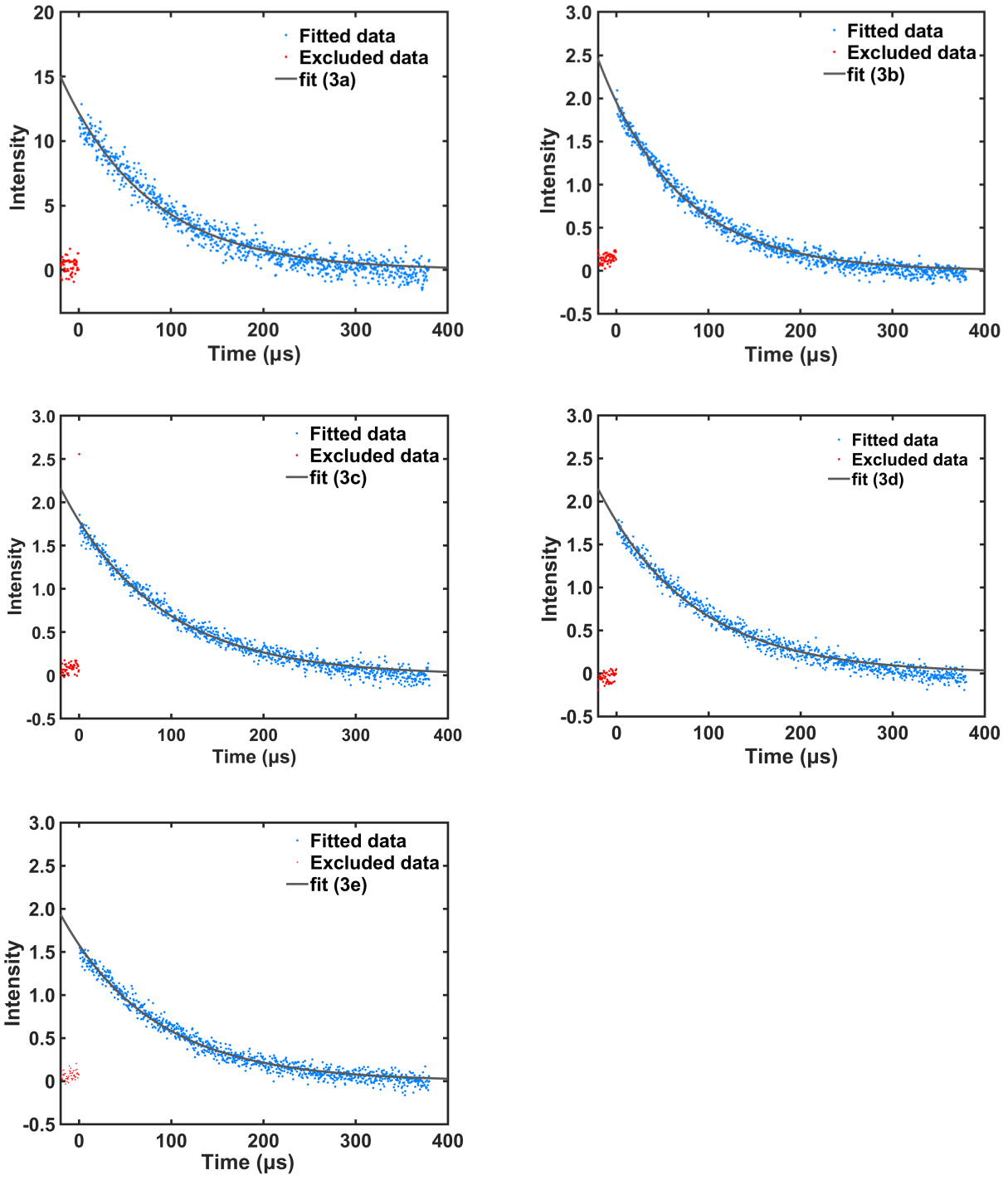


**Figure S5.** Time-resolved emission data for **3a**-**e** (conc. 15 μM). Phosphorescence monitored at 620 nm, $\lambda_{ex}$ = 355 nm, bandwidth = 5 nm.

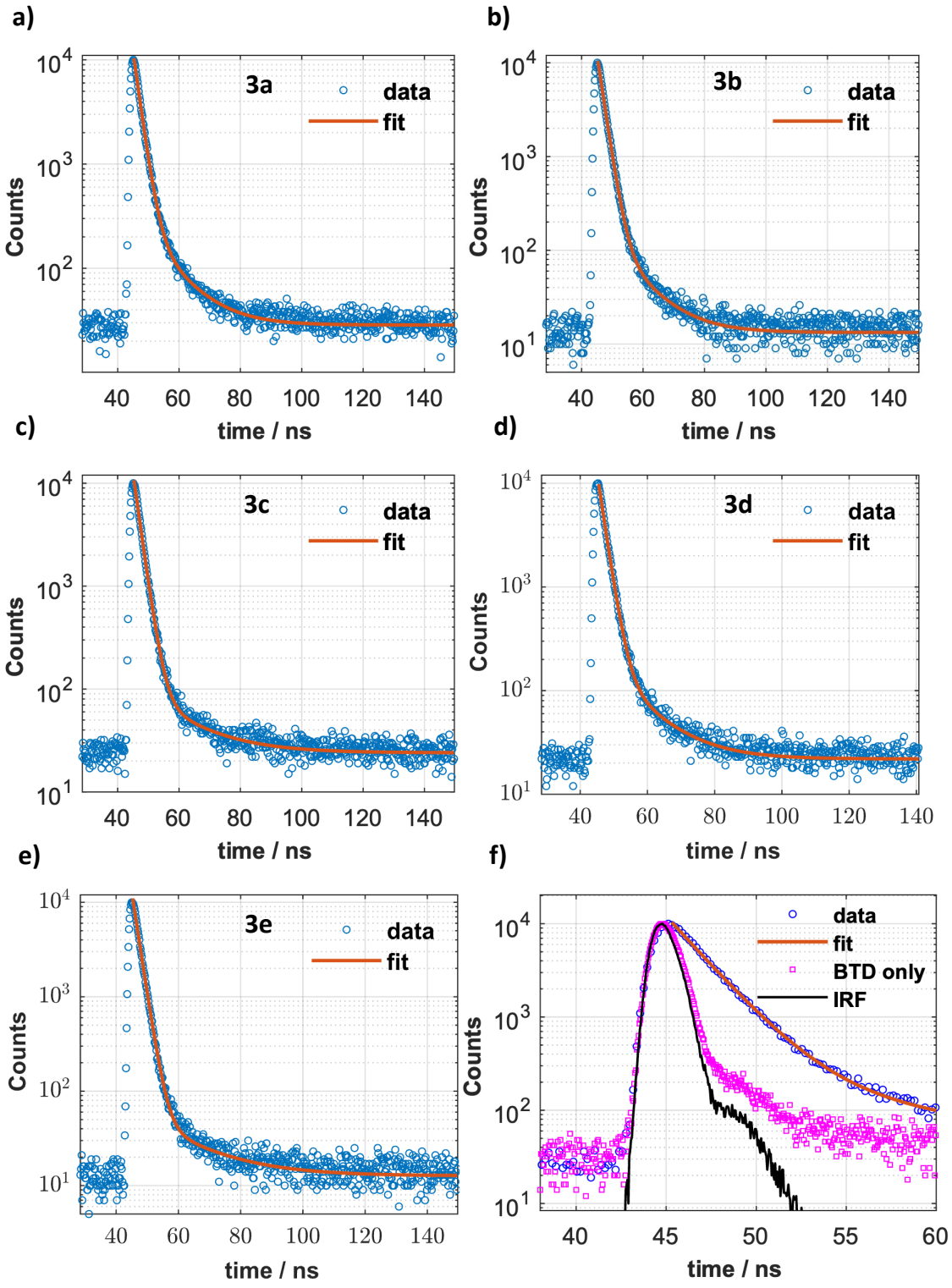


**Figure S6.** Panels a)-e): Time-correlated single photon counting (TCSPC) data for **3a**-**3e** monitored at 450 nm (fluorescence) recorded at room temperature in degassed 2-Me-THF (conc. 15 μM), $\lambda_{ex}$ = 341.3 nm, emission bandwidth = 10 nm. Panel f): Data for **3a** plotted together with the IRF (solid black line) and the fluorescence decay of BTD only (open pink squares). The latter is coincident with the IRF.

## IV. Computational results

### *Method validation by reproducing reported work.[10]*

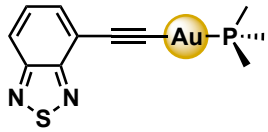


**Figure S7.** Complex investigated for method validation, **BTD–C≡C–Au–PMe$_3$** (compound **1a** from reference 10). Cyclohexyl moieties were truncated to methyl groups to expedite computational time.

**Table S3.** Table S5 from Ref. 10. Vertical excitation energies to singlet and triplet excited states and their corresponding compositions at the optimized $S_0$ geometry **BTD–C≡C–Au–PMe$_3$** by TD-DFT.[10]

| Transition | E (cm$^{-1}$) | λ (nm) | *f* | Major contribution | Minor contribution |
|---|---|---|---|---|---|
| T1 | 14642 | 683 | 0 | HOMO → LUMO (89%) | HOMO-4 → LUMO (7%) |
| S1 | 25237 | 396 | 0.2736 | HOMO → LUMO (99%) | - |
| T2 | 25811 | 387 | 0 | HOMO-3 → LUMO (89%) | HOMO → LUMO+1 (6%) |
| T3 | 27681 | 361 | 0 | HOMO-4 → LUMO (43%) | HOMO-3 → LUMO (7%) |
| | | | | HOMO → LUMO+1 (28%) | |
| T4 | 28417 | 352 | 0 | HOMO-1 → LUMO (90%) | HOMO-8 → LUMO (3%) |
| | | | | | HOMO-1 → LUMO+1 (2%) |
| S2 | 29464 | 339 | 0 | HOMO-1 → LUMO (97%) | HOMO-1 → LUMO+1 (2%) |

Employing computational details from the methods section, **BTD–C≡C–Au–PMe$_3$** was successfully optimized, yielding a structure with a singlet ground state ($S_0$). This wavefunction is stable and contains no imaginary frequencies (Lowest frequency: 14.722 cm$^{-1}$).

**Table S4.** Vertical excitation energies to singlet and triplet excited states and their corresponding compositions at the optimized $S_0$ geometry of **BTD–C≡C–Au–PMe$_3$** by TD-DFT. (This work).

| Transition | E (cm$^{-1}$) | λ (nm) | *f* | Major contribution | Minor contribution |
|---|---|---|---|---|---|
| T1 | 14636 | 683.27 | 0 | HOMO → LUMO (67%) | HOMO-4 → LUMO (19%) |
| S1 | 25211 | 396.66 | 0.2686 | HOMO → LUMO (70%) | - |
| T2 | 25822 | 387.26 | 0 | HOMO-3 → LUMO (67%) | HOMO → LUMO+1 (17%) |
| T3 | 27695 | 361.08 | 0 | HOMO-4 → LUMO (47%) | HOMO-3 → LUMO (18%) |
| | | | | HOMO → LUMO+1 (37%) | |
| T4 | 28387 | 352.28 | 0 | HOMO-1 → LUMO (67%) | HOMO-1 → LUMO+1 (12%) |
| S2 | 29434 | 339.74 | 0 | HOMO-1 → LUMO (70%) | - |

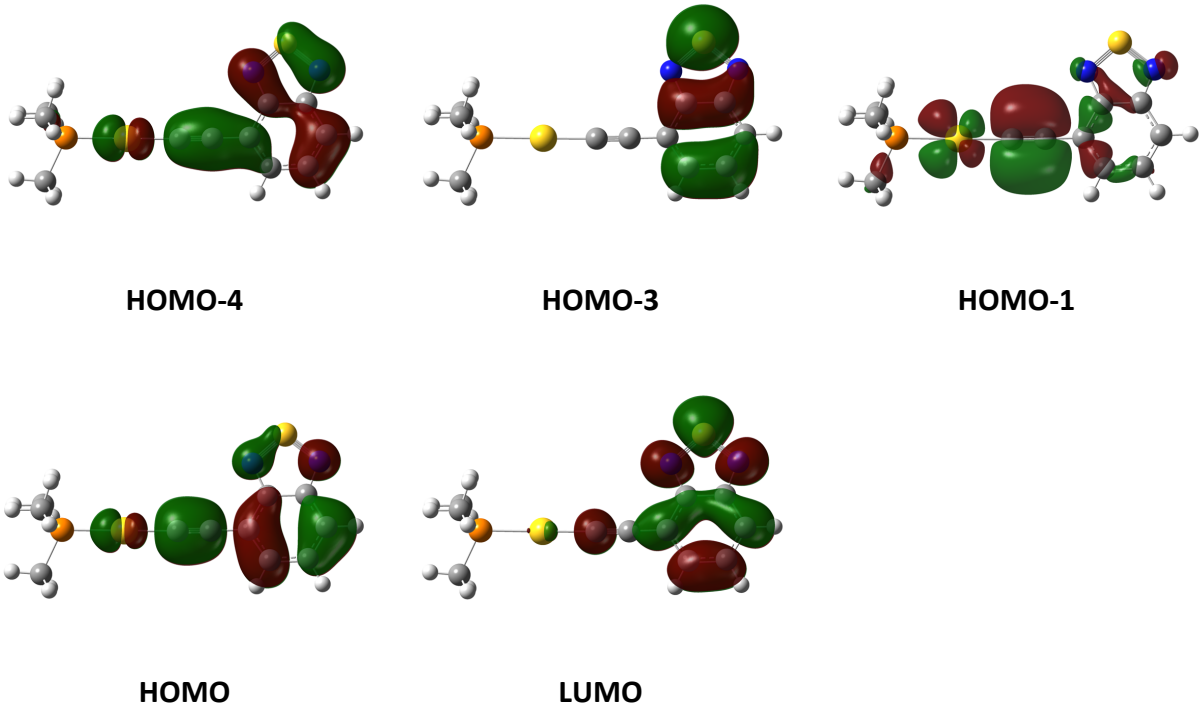


**Figure S8.** Select frontier MO surfaces (Isovalue: 0.02) at the optimized $S_0$ geometries of **BTD–C≡C–Au–PMe$_3$**.

**Conclusion:** Although minor discrepancies were observed in the TD-DFT results (i.e., vertical excitation energies, oscillator strength), the method used in these calculations yielded results that match well to those found in reference 10. The frontier orbitals associated with the predicted transitions also match well to those found in Table S9 of reference 10.

***Calculation of BTD-Au-PMe$_3$:***

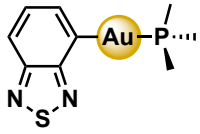


Cyclohexyl moieties were truncated to methyl groups to expedite computational time.[10] Attempts to optimize the full complex containing $PCy_3$ lead to results with imaginary frequencies (i.e., the computed structure is not at a potential surface minimum).

Employing computational details from the methods section, **BTD–Au–PMe$_3$** was successfully optimized, yielding a structure with a singlet groundstate ($S_0$). This wavefunction is stable and contains no imaginary frequencies (Lowest frequency: 16.398 $cm^{-1}$).

**Table S5.** Vertical excitation energies to singlet and triplet excited states and their corresponding compositions at the optimized $S_0$ geometry of **BTD–Au–PMe$_3$** by TD-DFT.

| Transition | E ($cm^{-1}$) | λ (nm) | *f* | Major contribution | Minor contribution |
|---|---|---|---|---|---|
| T1 | 16887 | 592.16 | 0 | HOMO → LUMO (69%) | HOMO-8 → LUMO (12%) |
| T2 | 25990 | 384.76 | 0 | HOMO-2 → LUMO (70%) | |
| T3 | 28566 | 350.07 | 0 | HOMO-1 → LUMO (69%) | HOMO-5 → LUMO (12%) |
| S1 | 29221 | 342.22 | 0.1238 | HOMO → LUMO (70%) | - |
| S2 | 30381 | 329.15 | 0.0010 | HOMO-1 → LUMO (70%) | |
| T4 | 32142 | 311.12 | 0 | HOMO → LUMO+1 (41%) | |
| | | | | HOMO-10 → LUMO (34%) | |
| | | | | HOMO → LUMO+6 (32%) | |

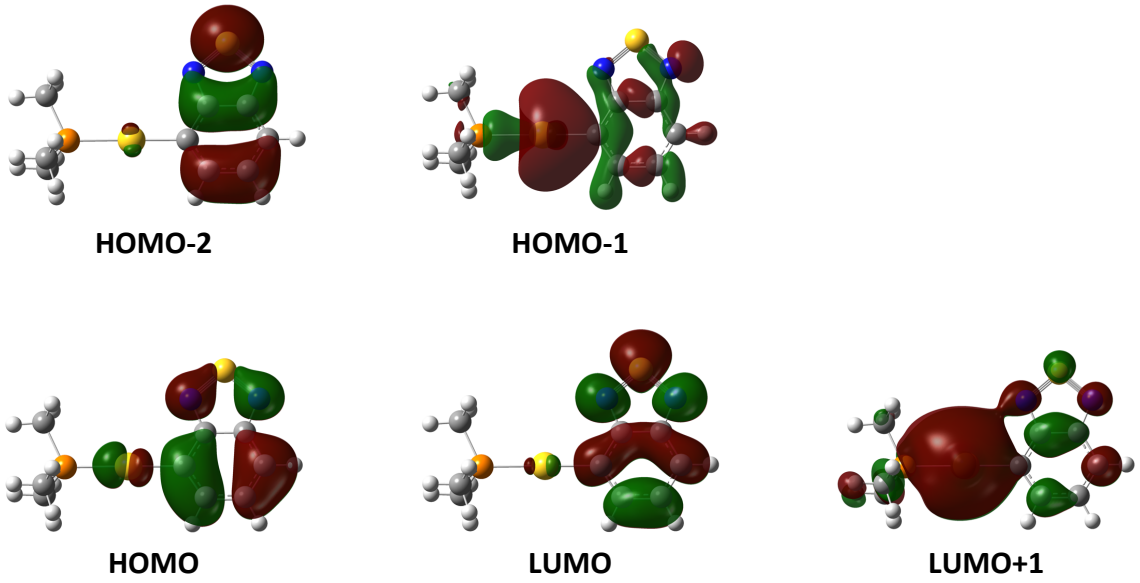


**Figure S9.** Selecteded frontier MO surfaces (Isovalue: 0.02) at the optimized $S_0$ geometries of **BTD–Au–PMe$_3$**.

Similar to **BTD–C≡C–Au–PMe$_3$**, the HOMO and LUMO of **BTD–Au–PMe$_3$** are predominantly localized on the benzothiadiazole ligand with minimal contribution from the phosphine. Both orbitals are comprised of antibonding combinations of an Au(d) orbital with the π-system of BTD.

***Conclusion:*** Removing the acetylide moiety (**BTD–C≡C–Au–PMe$_3$** *vs* **BTD–Au–PMe$_3$**) yields a 4000 cm$^{-1}$ blue shift in the calculated vertical excitation energies.

***Calculation of BTD-Au-IPr (3d):***

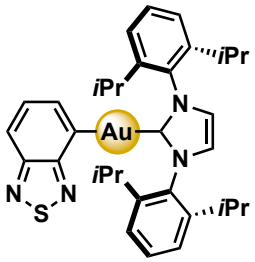


Employing computational details from the methods section, BTD–Au–IPr (**3d**) was successfully optimized, yielding a structure with a singlet ground state ($S_0$). This wavefunction is stable and contains no imaginary frequencies (Lowest frequency: 12.0376 $cm^{-1}$).

**Table S6.** Vertical excitation energies to singlet and triplet excited states and their corresponding compositions at the optimized $S_0$ geometry of BTD–Au–IPr (**3d**) by TD-DFT.

| Transition | E ($cm^{-1}$) | λ (nm) | *f* | Major contribution | Minor contribution |
|---|---|---|---|---|---|
| T1 | 16730 | 597.73 | 0 | HOMO → LUMO (0.68) | HOMO-12 → LUMO (0.10) |
| T2 | 26040 | 384.02 | 0 | HOMO-4 → LUMO (0.70) | - |
| T3 | 28343 | 352.82 | 0 | HOMO-1 → LUMO (0.65) | HOMO-7 → LUMO (0.15) |
| T4 | 28500 | 350.88 | 0 | HOMO-2 → LUMO+5 | |
| T5 | 28501 | 350.86 | 0 | | |
| S1 | 28702 | 348.41 | 0.1289 | HOMO → LUMO (0.70) | |

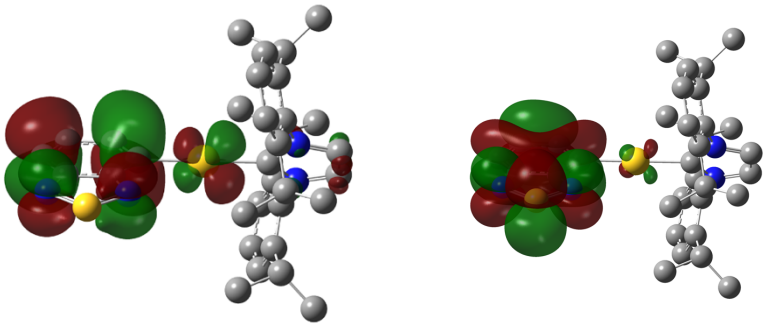

**HOMO** **LUMO**

**Figure S10.** Selected frontier MO surfaces (Isovalue: 0.02) at the optimized $S_0$ geometries of BTD–Au–IPr (**3d**).

***Calculation of BTD-Au-IMes:***

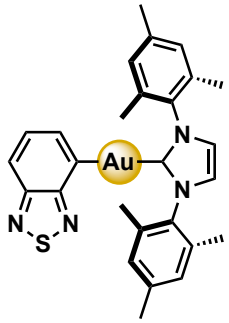


Employing computational details from the general methods section, **BTD–Au–NHCMe$_3$** was successfully optimized, yielding a structure with a singlet ground state ($S_0$). This wavefunction is stable and contains no imaginary frequencies (Lowest frequency: 5.9913 cm$^{-1}$).

**Table S7.** Vertical excitation energies to singlet and triplet excited states and their corresponding compositions at the optimized $S_0$ geometry of BTD–Au–IMes (**3e**) by TD-DFT.

| Transition | E (cm$^{-1}$) | λ (nm) | *f* | Major contribution | Minor contribution |
|---|---|---|---|---|---|
| T1 | 16746 | 597.16 | 0 | HOMO → LUMO (0.68) | HOMO-12 → LUMO (0.13) |
| T2 | 26028 | 384.20 | 0 | HOMO-6 → LUMO (0.70) | - |
| T3 | 28399 | 352.13 | 0 | HOMO-2 → LUMO+2 (0.38) | |
| T4 | 28416 | 351.92 | 0 | HOMO-2 → LUMO+3 (0.37) | |
| T5 | 28528 | 350.53 | 0 | HOMO-1→ LUMO (0.62) | HOMO-7 → LUMO (0.17) |
| S1 | 28807 | 347.14 | 0.1160 | HOMO → LUMO (0.70) | - |

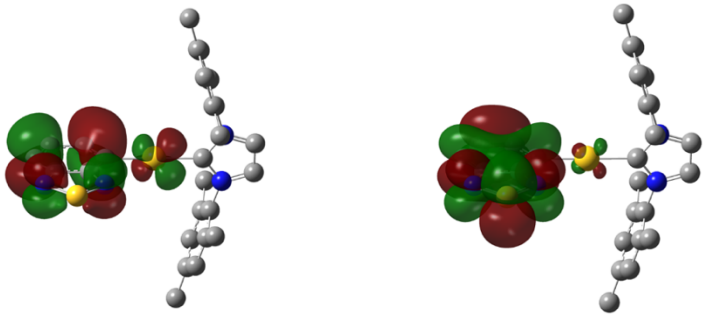

**HOMO** **LUMO**

**Figure S11.** Selected frontier MO surfaces (Isovalue: 0.02) at the optimized $S_0$ geometries of BTD–Au–IMes (**3e**).

***Conclusion:*** The predicted vertical excitation energies for BTD–Au–IPr (**3d**) and BTD–Au–IMes (**3e**) occurs between the HOMO and LUMO. Their orbitals are similar in composition to those found in **BTD–Au–PMe$_3$**, comprising of antibonding combinations of a Au(d) orbital with the π-system of BTD.

## V. Electrochemical data

### *Cyclic voltammograms of BTD–Au–PPh₃:*

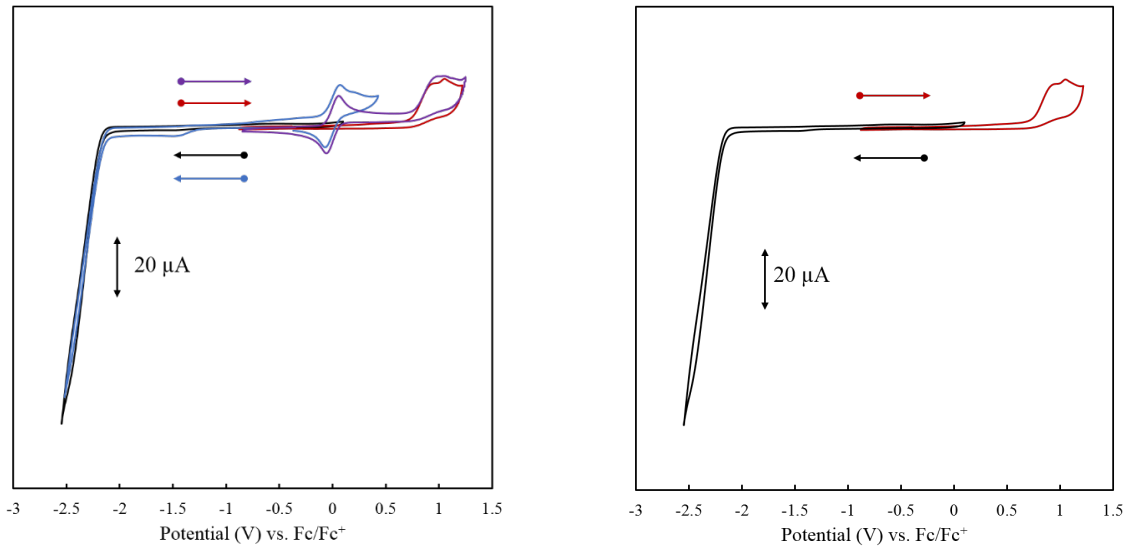


**Figure S12.** CVs of **BTD–Au–PPh₃** (**3a**) in THF containing ferrocene internal standard (left) and without internal standard (right).

**Table S8.** Redox potentials of **BTD–Au–PPh₃** (**3a**) in THF versus $Fc^+/Fc$.

| Redox Values of **3a** | |
|---|---|
| Event | Potential (V) |
| $E_1$ | 0.95 |
| $E_2$ | 1.05 |

***Cyclic voltammograms of BTD–Au–P$^t$Bu$_3$ (3b):***

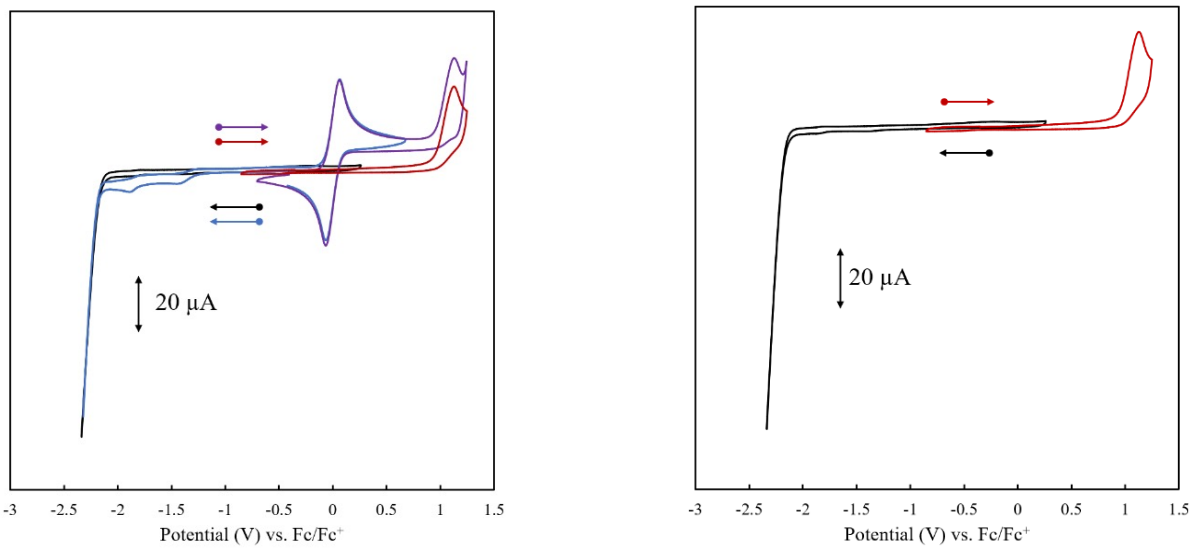


**Figure S13.** CVs of **BTD–Au–PtBu$_3$** (**3b**) in THF containing ferrocene internal standard (left) and without internal standard (right).

**Table S9.** Redox potentials of **BTD–Au–PtBu$_3$** (**3b**) in THF versus $Fc^+$/Fc.

| Redox Values of **3b** | |
|---|---|
| Event | Potential (V) |
| $E_1$ | -2.34 |
| $E_2$ | 1.13 |

***Cyclic voltammograms of BTD–Au–PCy₃ (3c):***

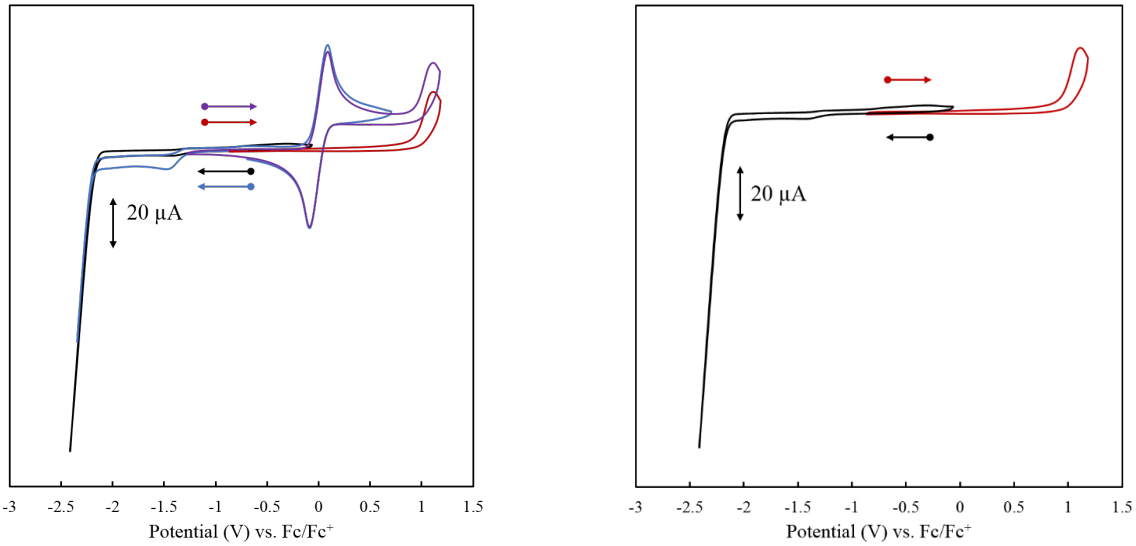


**Figure S14.** CVs of BTD–Au–$PCy_3$ (**3c**) in THF containing ferrocene internal standard (left) and without internal standard (right).

**Table S10.** Redox potentials of BTD–Au–$PCy_3$ (**3c**) in THF versus $Fc^+/Fc$.

| Redox Values of **3c** | |
|---|---|
| Event | Potential (V) |
| $E_1$ | -2.41 |
| $E_2$ | 1.11 |

***Cyclic voltammograms of BTD–Au–IPr (3d):***

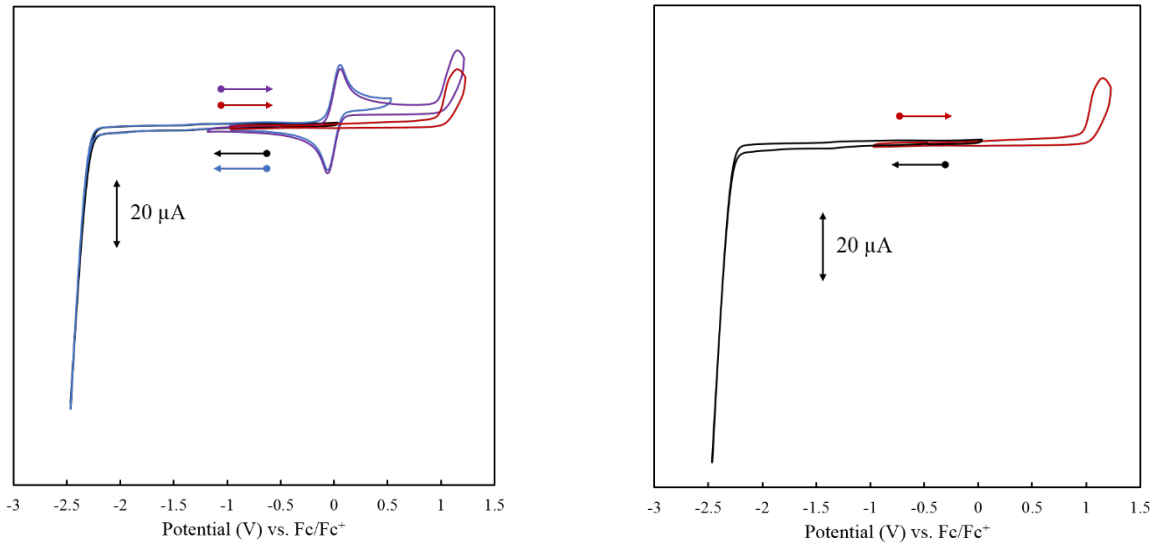


**Figure S15.** CVs of BTD–Au–IPr (**3d**) in THF containing ferrocene internal standard (left) and without internal standard (right).

**Table S11.** Redox potentials of BTD–Au–IPr (**3d**) in THF versus $Fc^+/Fc$.

| Redox Values of **3d** | |
|---|---|
| Event | Potential (V) |
| $E_1$ | -2.46 |
| $E_2$ | 1.15 |

***Cyclic voltammograms of BTD–Au–IMes (3e):***

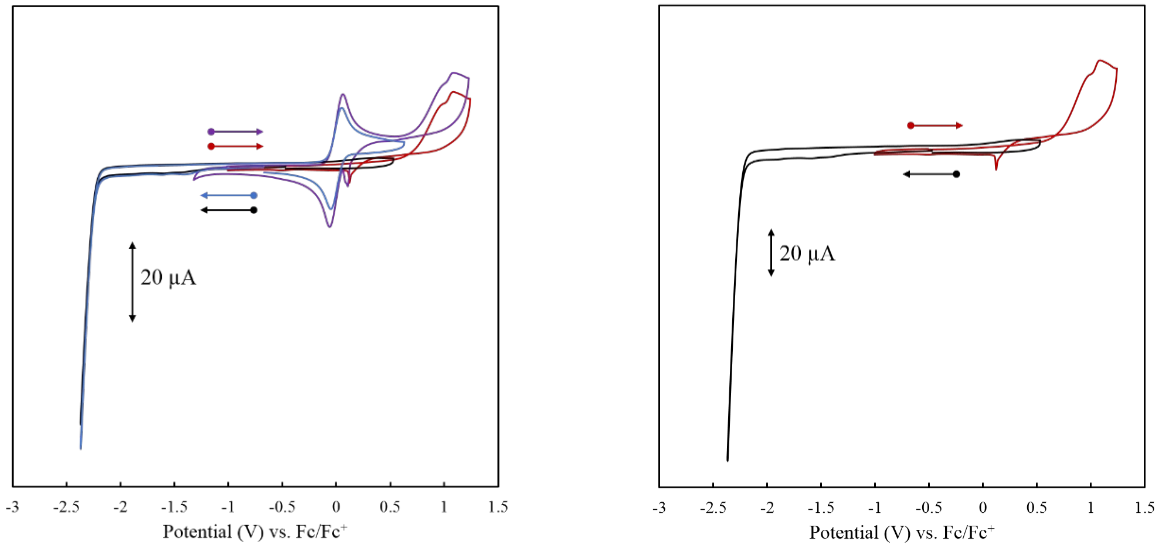


**Figure S16.** CV of BTD–Au–IPr (**3e**) in THF containing ferrocene internal standard (left) and without internal standard (right).

**Table S12.** Redox potentials of BTD–Au–IPr (**3e**) in THF versus $Fc^{+}/Fc$.

| Redox Values of **3e** | |
|---|---|
| Event | Potential (V) |
| $E_1$ | -2.37 |
| $E_2$ | 0.93 |
| $E_3$ | 1.09 |

## VI. Crystallographic details

The complexes all exhibit linear two-coordinate geometry; the phosphine complexes exhibit C1–Au–P1 angles closer to the ideal arrangement than the C1–Au–C7 angles of the *N*-heterocyclic carbene complexes (177.79(6) – 178.92(10)° versus 166.6(4) – 175.01(13)°), due to the larger steric bulk at the metal centre imposed by the NHC ligands. The Au1–P1, Au1–C1, and Au1–C7 distances are comparable to those of related Au(I) complexes. The Au–C1 and Au–C7 bonds in **3d** are slightly elongated when compared to **3e** (Au–C1: 2.086(4) and 2.052(4) Å; Au–C7: 2.3172(8) and 2.2954(10) Å respectively), likely due to the greater steric demand of the IPr ligand compared to the IMes ligand. The Au–C and Au–P bonds decrease in the order $PtBu_3$>$PCy_3$>$PPh_3$ (Au-C: 2.086(4), 2.052(4), and 2.0455(17) Å; Au-P: 2.3172(8), 2.2954(10), and 2.2845(5) Å, respectively), which is consistent with the decreasing σ-donation strength of the phosphine ligand. The Au–C and Au–P bonds are shortest for the $PPh_3$ ligand, which is the weakest σ-donating ligand, and strongest pi-acceptor.

Specific for **3a** ($PPh_3$ ligand): No additional information.
Specific for **3b** ($P^tBu_3$ ligand): The gold centre, the benzothiadiazole ligand, and one of the phosphine tertiary butyl groups are disordered along a crystallographic mirror plane.
Specific for **3c** ($PCy_3$ ligand): There is a positional disorder of the gold centre and the benzothiadiazole ligand.
Specific for **3d** (IPr ligand): There is a positional disorder of one of the NHC isopropyl groups.
Specific for **3e** (IMes ligand**)**: There are two molecules of **3e** in the unit cell. One of these molecules exhibits a positional disorder for the benzothiadiazole ligand over two sites.

CCDC 2026788 and 2125287-2125290 contain the supplementary crystallographic data for this paper. The data can be obtained free of charge from The Cambridge Crystallographic Data Centre via www.ccdc.cam.ac.uk/structures.

**Table S13.** Crystal data and structure refinement for **3a**-**e**.

| *Compound* | **3a** ($PPh_3$) | **3b** ($P^tBu_3$) | **3c** ($PCy_3$) | **3d** (IPr) | **3e** (IMes) |
|---|---|---|---|---|---|
| **Chemical formula** | $C_{24}H_{18}AuN_2PS$ | $C_{18}H_{30}AuN_2PS$ | $C_{24}H_{36}AuN_2PS$ | $C_{33}H_{39}AuN_4S$ | $C_{27}H_{27}AuN_4S$ |
| $M_r$ | 590.40 | 534.43 | 612.54 | 720.71 | 636.55 |
| **Crystal system, space group** | Monoclinic<br>$P2_1/c$ | Monoclinic<br>$P2_1/m$ | Triclinic<br>$P\bar{1}$ | Monoclinic<br>$P2_1/c$ | Triclinic<br>$P\bar{1}$ |
| **Temperature (K)** | 170 | 170 | 170 | 170 | 170 |
| ***a*, *b*, *c* (Å)** | 8.4960(4)<br>11.3452(6)<br>21.6600(11) | 8.4072(2)<br>13.1964(4)<br>9.2110(2) | 9.4554(4)<br>11.6097(6)<br>11.8845(5) | 11.819(2)<br>14.047(3)<br>18.837(3) | 10.3239(4)<br>15.6203(6)<br>16.6809(7) |
| **a, b, g (°)** | -<br>97.820(1)<br>- | -<br>93.753(1)<br>- | 96.835(1)<br>111.00(3)<br>94.095(1) | -<br>96.458(4)<br>- | 105.253(1)<br>100.318(1)<br>102.032(1) |
| ***V* (Å$^3$)** | 2068.37 | 1019.72(5) | 1200.09(10) | 3107.5(9) | 2458.97(17) |
| ***Z*** | 4 | 2 | 2 | 4 | 4 |
| **Radiation type** | Mo Ka | Mo Ka | Mo Ka | Mo Ka | Mo Ka |
| **m (mm$^{-1}$)** | 7.30 | 7.4 | 6.3 | 4.83 | 6.09 |
| **Crystal size (mm)** | 0.25 × 0.20 × 0.10 | 0.30 × 0.30 × 0.07 | 0.6 × 0.4 × 0.3 | 0.20 × 0.09 × 0.09 | 0.22 × 0.19 × 0.12 |
| **Diffractometer** | Bruker D8 APEX-II | Bruker D8 APEX-II | Bruker D8 APEX-II | Bruker D8 APEX-II | Bruker D8 APEX-II |
| **Absorption correction** | Multi-scan | Multi-scan | Multi-scan | Multi-scan | Multi-scan |
| $T_{min}$, $T_{max}$ | 0.471, 0.746 | 0.436, 0.747 | 0.676, 0.749 | 0.474, 0.746 | 0.610, 0.746 |
| **No. of measured, independent and observed [I > 2σ(I)] reflections** | 59053<br>5612<br>5203 | 41113<br>4223<br>3291 | 53061<br>6700<br>6212 | 120163<br>7800<br>6957 | 133098<br>13393<br>11662 |
| $R_{int}$ | 0.028 | 0.054 | 0.042 | 0.064 | 0.037 |
| **(sin Θ/λ)$_{max}$ (Å$^{-1}$)** | 0.687 | 0.782 | 0.694 | 0.672 | 0.691 |
| ***R*[$F^2$ > 2s($F^2$)], *wR*($F^2$), *S*** | 0.014, 0.032, 1.03 | 0.030, 0.076, 1.03 | 0.016, 0.036, 1.06 | 0.018, 0.044, 1.05 | 0.024, 0.056, 1.06 |
| **No. of parameters** | 262 | 150 | 353 | 406 | 665 |
| **No. of restraints** | 0 | 0 | 176 | 39 | 686 |
| **H-atom treatment** | Constrained | Constrained | Constrained | Constrained and independent | Constrained |
| **Δ>$_{max}$, Δ>$_{min}$ (e Å$^{-3}$)** | 0.77, -0.35 | 1.03, -1.02 | 0.45, -0.66 | 0.68, -0.70 | 2.16, -1.69 |
| **CCDC No.** | 2125288 | 2125287 | 2026788 | 2125289 | 2125290 |

Pale yellow crystals of **3a** suitable of single crystal X-ray diffraction were grown by slow diffusion of pentane into a concentrated $CH_2Cl_2$ solution of **3a**. Compound **3a** crystallises in the monoclinic space group $P2_1/c$. The solid-state structure shows a two coordinate Au centre, coordinated to a phosphine and an aryl ligand. The arrangement is near linear with an angle of 177.79°. The Au-P and Au-C are comparable to other gold(I) aryl phosphine complexes.

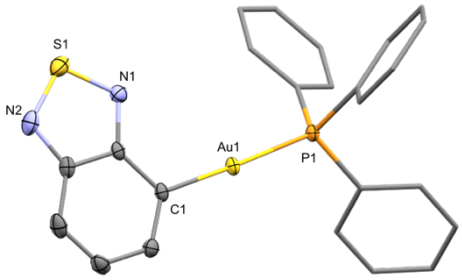


**Figure S17.** Solid-state structure of **3a**. Ellipsoids at 50% probability, methyl groups as capped sticks and hydrogen atoms removed for clarity. Selected metrics: Au1–C1: 2.0455(17) Å; Au1–P1: 2.2845(5) Å; C1–Au1–P1: 177.79(6)°.

Pale yellow crystals of **3b** suitable of single crystal X-ray diffraction were grown by slow diffusion of pentane into a concentrated $CH_2Cl_2$ solution of **3b**. Compound **3b** crystallises in the monoclinic space group $P2_1/m$. The solid-state structure shows a two coordinate Au centre, coordinated to a phosphine and an aryl ligand. The arrangement is near linear with an angle of 178.92°. The Au-P and Au-C are comparable to other gold(I) aryl phosphine complexes.

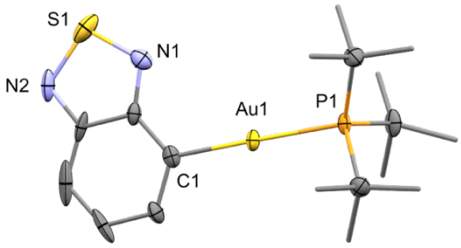


**Figure S18.** Solid-state structure of **3b**. Ellipsoids at 50% probability, methyl groups as capped sticks and hydrogen atoms removed for clarity. Selected metrics: Au1–C1: 2.086(4) Å; Au1-P1: 2.3172(8) Å; C1–Au1–P1: 178.92(10)°.

Pale yellow crystals of **3c** suitable of single crystal X-ray diffraction were grown by slow diffusion of pentane into a concentrated $CH_2Cl_2$ solution of **3c**. Compound **3c** crystallises in the triclinic space group P–1. The solid-state structure shows a two coordinate Au centre, coordinated to a phosphine and an aryl ligand. The arrangement is near linear with an angle of 177.90°. The Au–P and Au–C are comparable to other gold(I) aryl phosphine complexes.

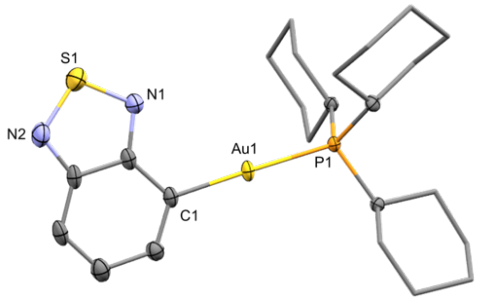


**Figure S19.** Solid-state structure of **3c**, (TK1901). Ellipsoids at 50% probability, methyl groups as capped sticks and hydrogen atoms removed for clarity. Selected metrics: Au1–C1: 2.052(4) Å; Au1–P1: 2.2954(10) Å; C1–Au1–P1: 177.90(9)°.

Pale yellow crystals of **3d** suitable of single crystal X-ray diffraction were grown by slow diffusion of pentane into a concentrated $CH_2Cl_2$ solution of **3d**. Compound **3d** crystallises in the monoclinic space group $P2_1/c$. The solid-state structure shows a two coordinate Au centre, coordinated to a NHC and an aryl ligand. The arrangement is near linear with an angle of 175.01°. The Au-$C_{NHC}$ and Au-$C_{aryl}$ bonds are comparable to other NHC gold(I) aryl complexes.

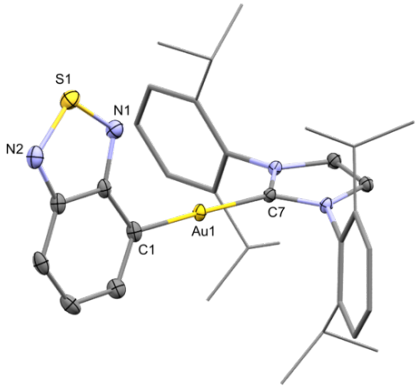


**Figure S20.** Solid-state structure of **3d**. Ellipsoids at 50% probability, methyl groups as capped sticks and hydrogen atoms removed for clarity. Selected metrics: Au1–C1: 2.035(2) Å; Au1–C7: 2.0260(18) Å; C1–Au1–C7: 175.01(8)°.

Pale yellow crystals of **3e** suitable of single crystal X-ray diffraction were grown by slow diffusion of pentane into a concentrated $CH_2Cl_2$ solution of **3e**. Compound **3e** crystallises in the triclinic space group P–1. The solid-state structure shows a two coordinate Au centre, coordinated to a NHC and an aryl ligand. The arrangement is near linear with an angle which ranges 166.64-174.09°. The Au–$C_{NHC}$ and Au–$C_{aryl}$ bonds are comparable to other NHC gold(I) aryl complexes.

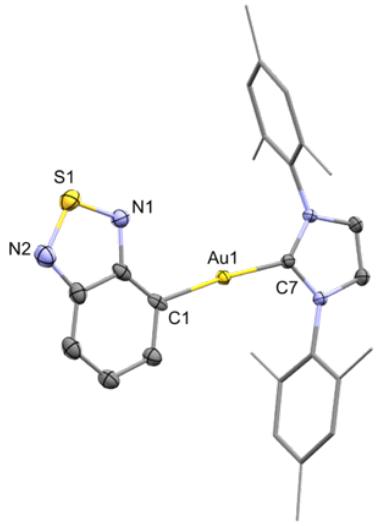


**Figure S21.** Solid-state structure of **3e**. Ellipsoids at 50% probability, methyl groups as capped sticks and hydrogen atoms removed for clarity. Selected metrics: Au1–C1: 2.099(3)-2.128(2) Å; Au1–C7: 2.019(3)-2.020(3) Å; C1–Au1–C7: 166.6(4)-174.09(13)°.

**Table S14.** Selected bond lengths (Å) and angles (°) for **3a**-**e**.

| **Compound** | **3a** | **3b** | **3c** | **3d** | **3e** |
|---|---|---|---|---|---|
| **L =** | $PPh_3$ | $P^tBu_3$ | $PCy_3$ | IPr | IMes |
| **Au-C1** | 2.0455(17) | 2.086(4) | 2.052(4) | 2.035(2) | 2.099(3) – 2.128(2) |
| **Au-P1** | 2.2845(5) | 2.3172(8) | 2.2954(10) | - | - |
| **Au-C7** | - | - | - | 2.0260(18) | 2.019(3) – 2.020(3) |
| **C1-Au-P1** | 177.79(6) | 178.92(10) | 177.90(9) | - | - |
| **C1-Au-C7** | - | - | - | 175.01(8) | 166.6(4) – 174.09(13) |

## VII. NMR Spectra

$^{1}$H NMR (400 MHz, $C_6D_6$) for 2,1,3-benzothiadiazole (BTD).

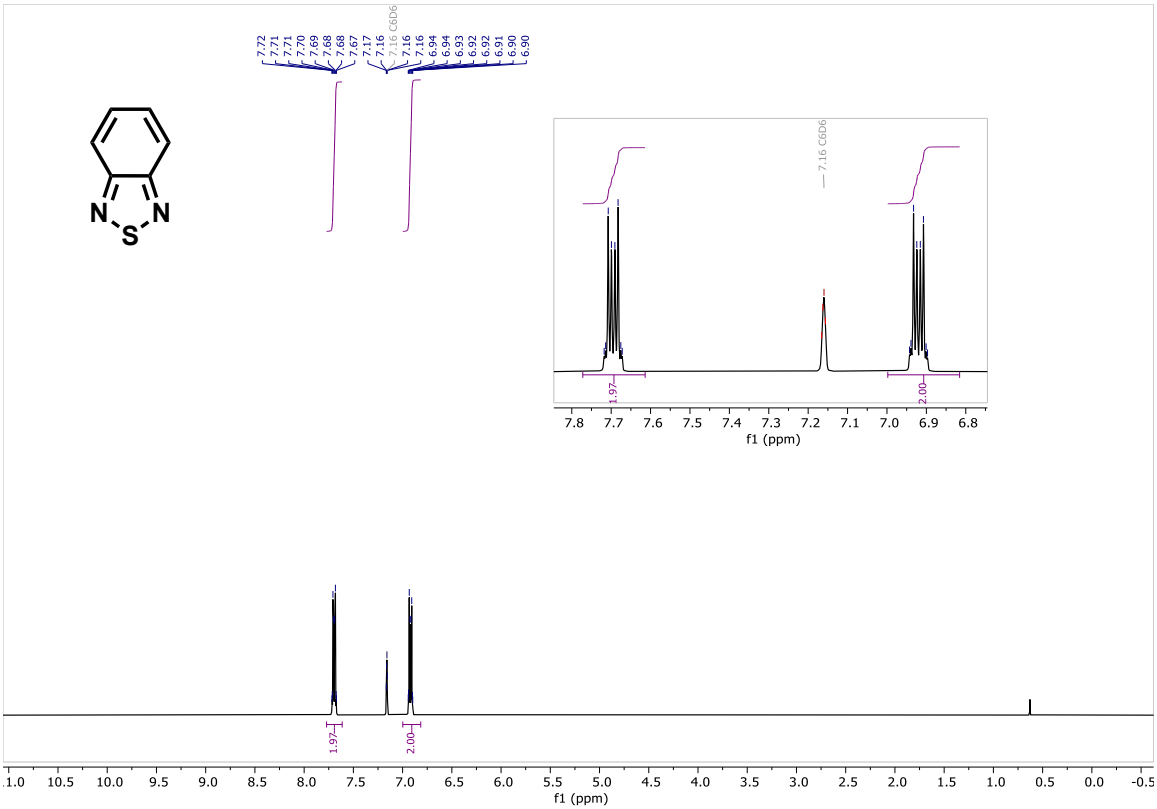


$^{13}$C NMR (101 MHz, $C_6D_6$) for 2,1,3-benzothiadiazole (BTD).

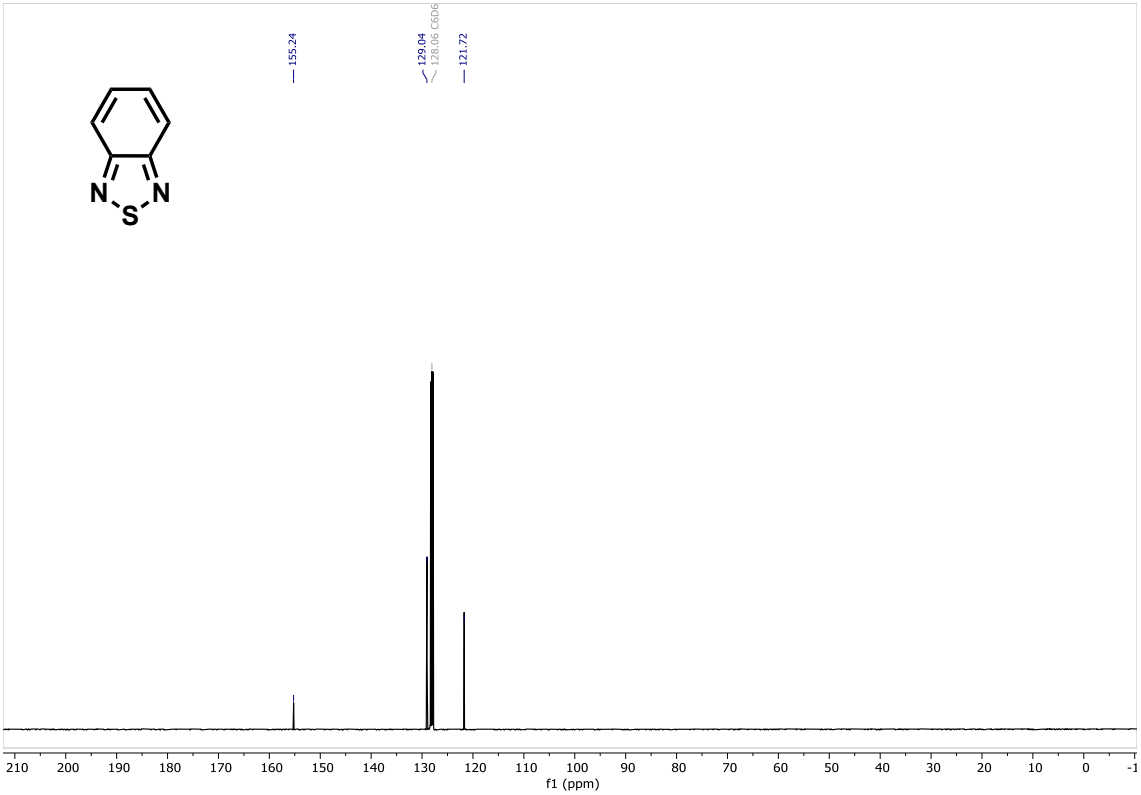

$^{1}$H NMR (400 MHz, $CDCl_3$) for compound **2**.

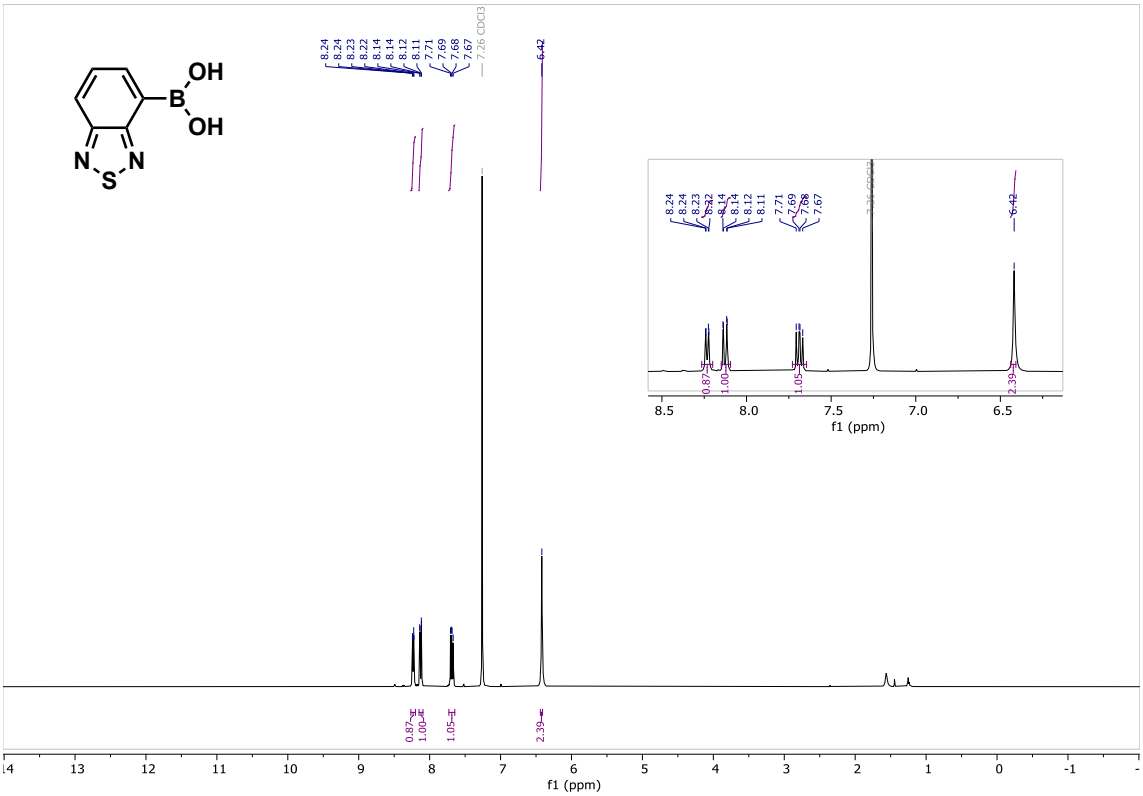


$^{13}$C NMR (101 MHz, $CDCl_3$) for compound **2**.

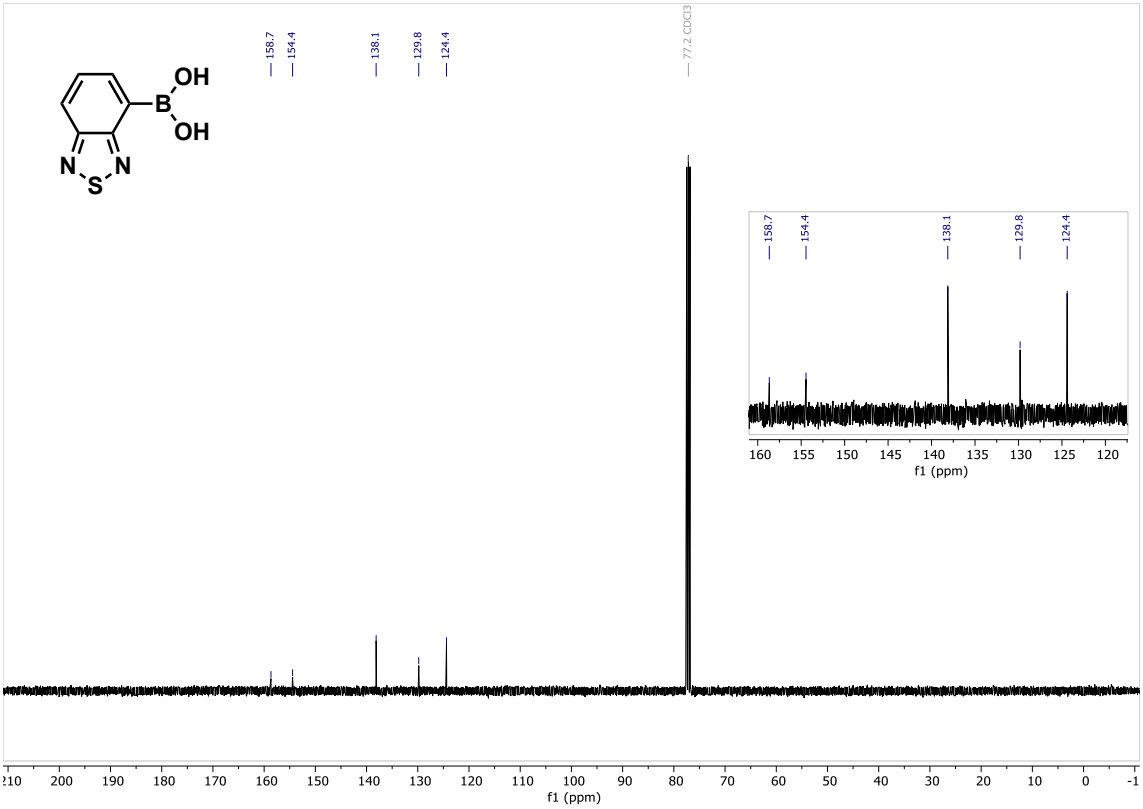

$^{11}B$ NMR (128 MHz, $CDCl_3$) for compound **2**.

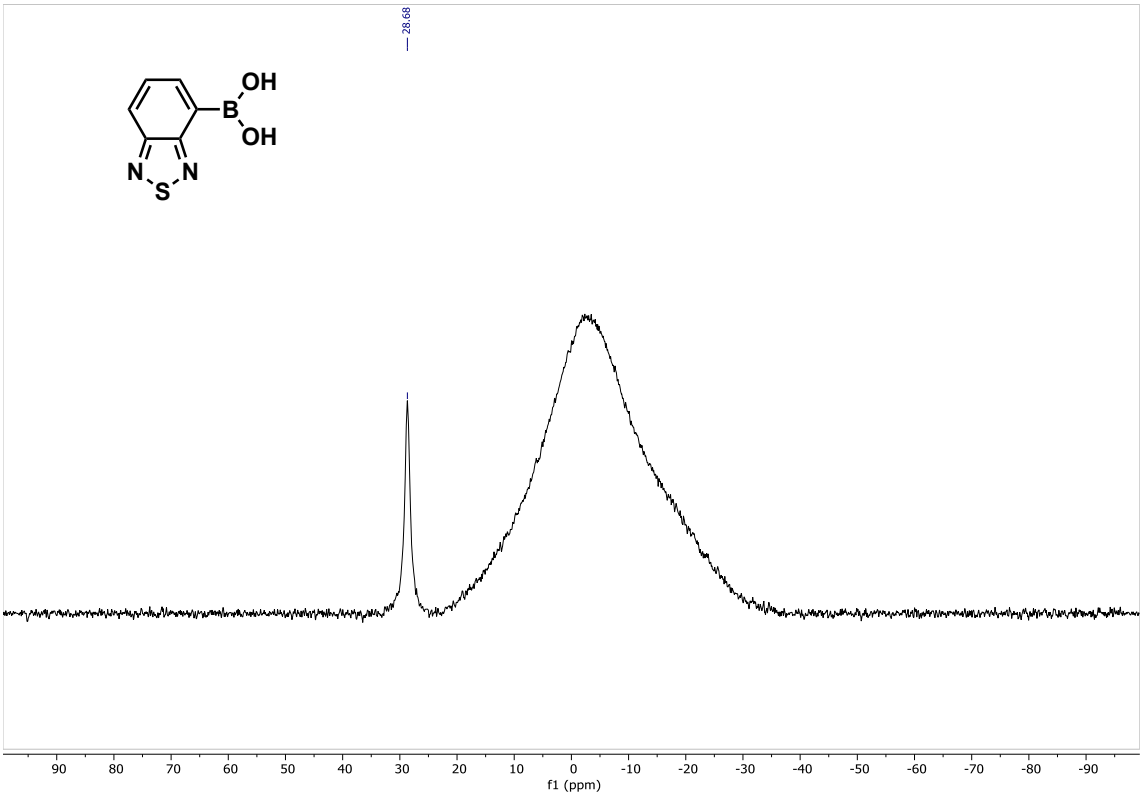


$^{1}H$ NMR (400 MHz, $C_6D_6$) for compound **3a**.

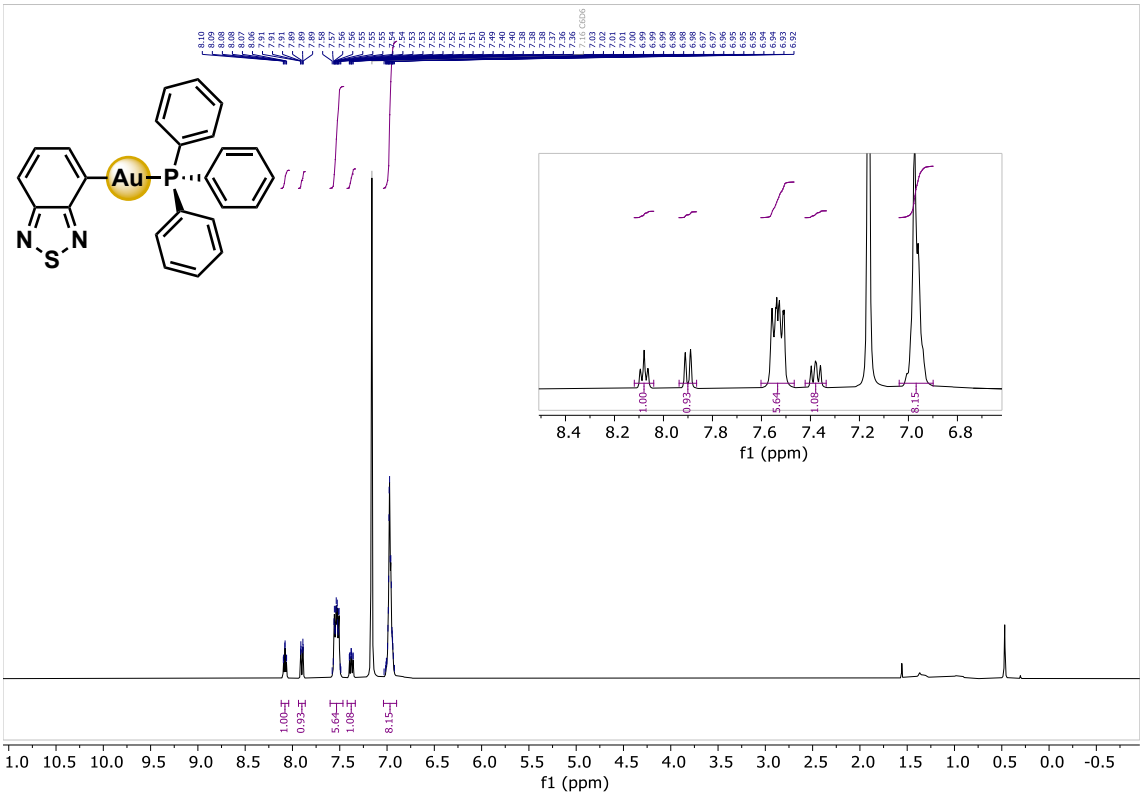

$^{13}C$ NMR (101 MHz, $C_6D_6$) for compound **3a**.

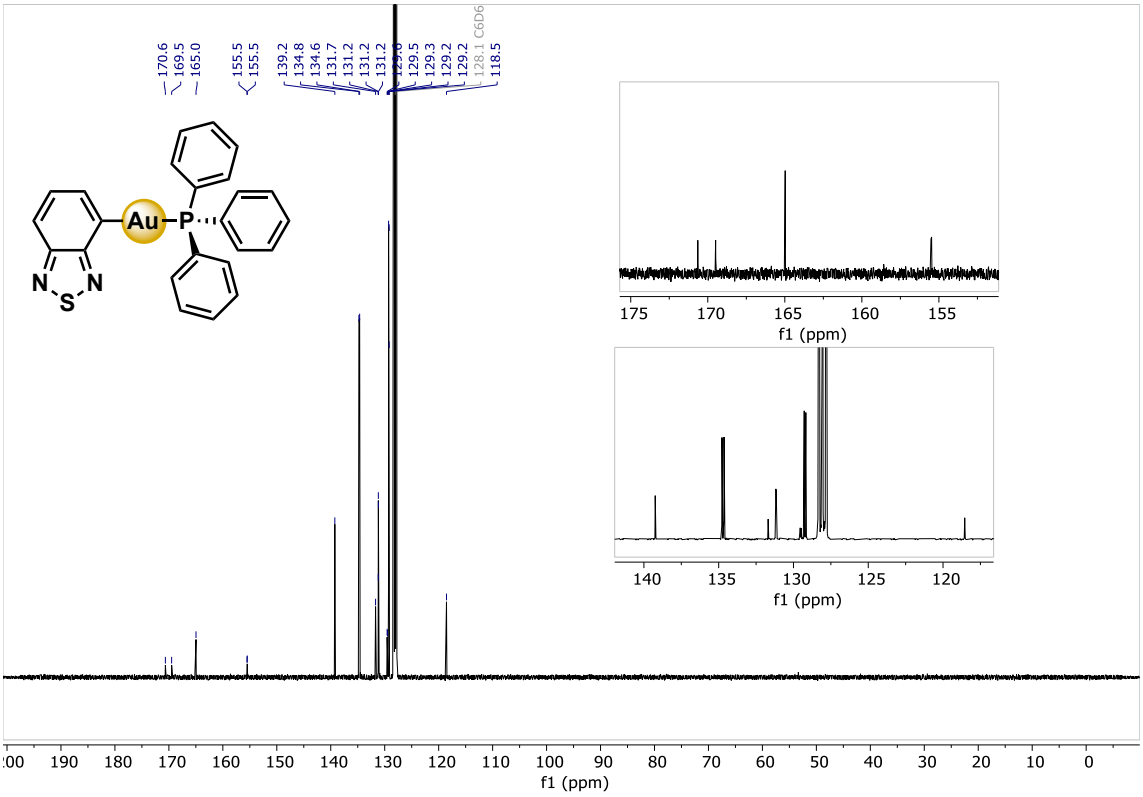


$^{31}P$ NMR (162 MHz, $C_6D_6$) for compound **3a**.

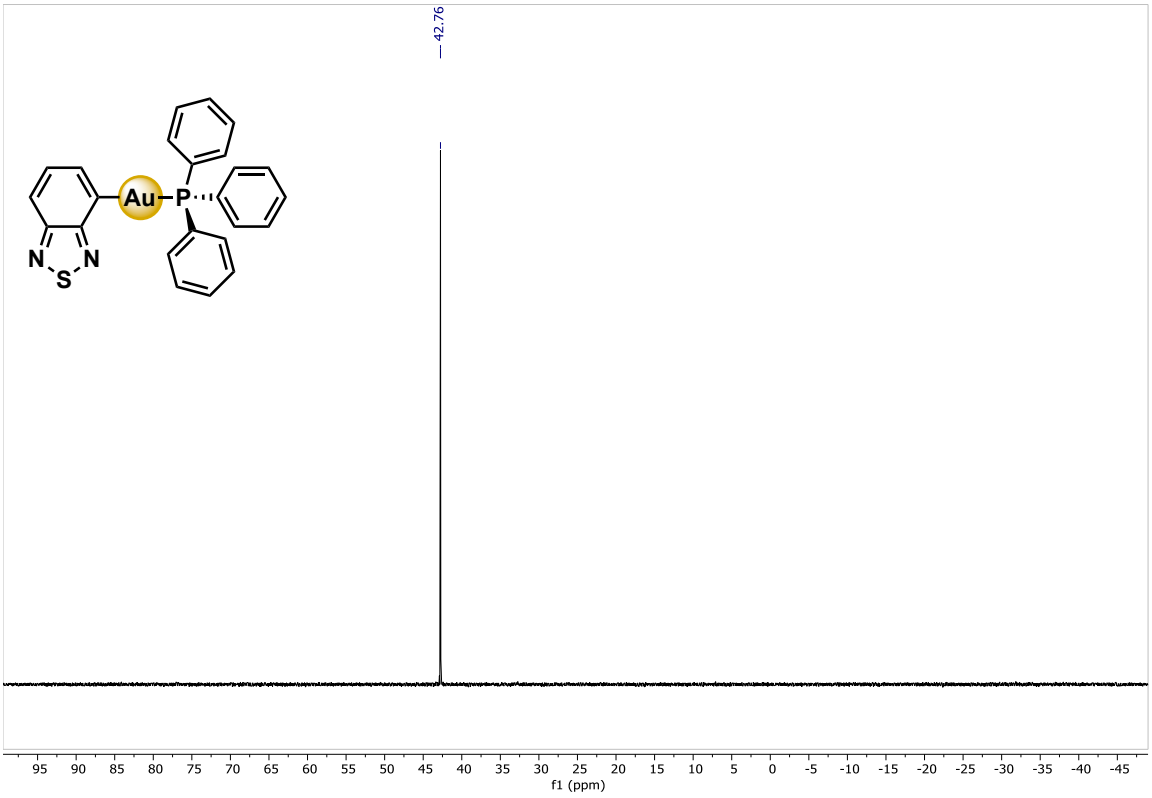

$^{1}$H NMR (400 MHz, $C_6D_6$) for compound **3b**.

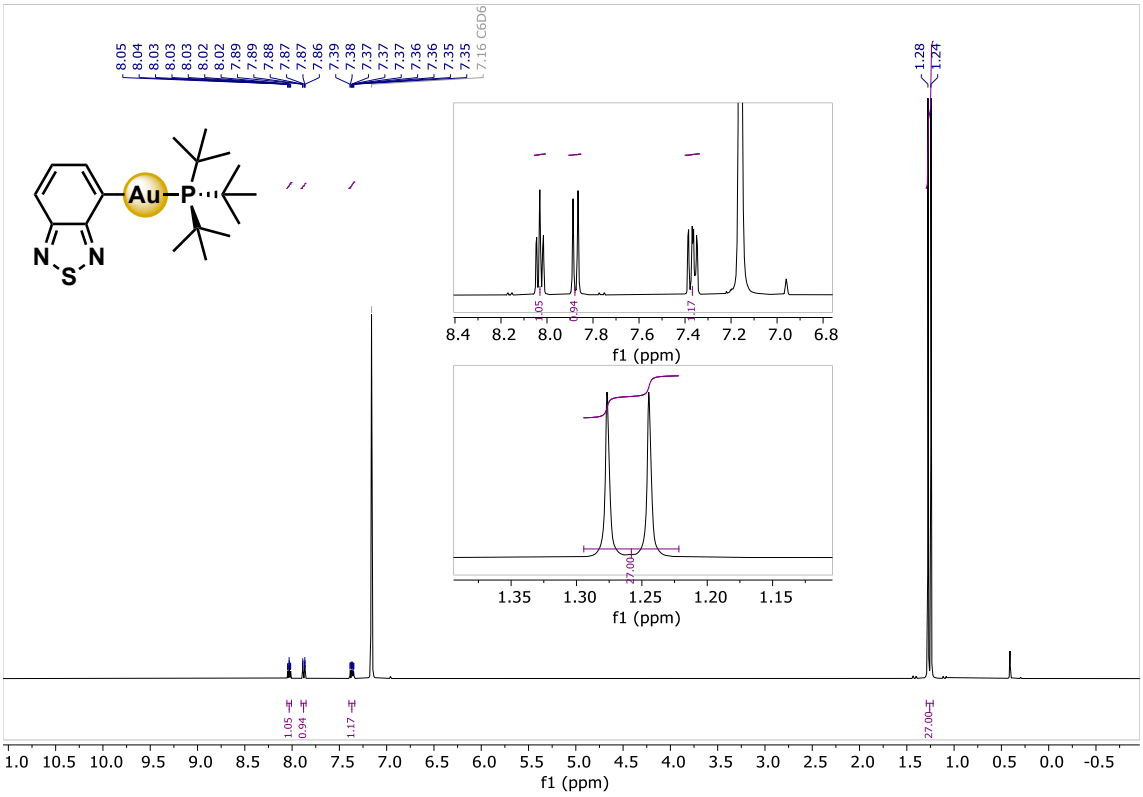


$^{13}$C NMR (101 MHz, $CDCl_3$) for compound **3b**.

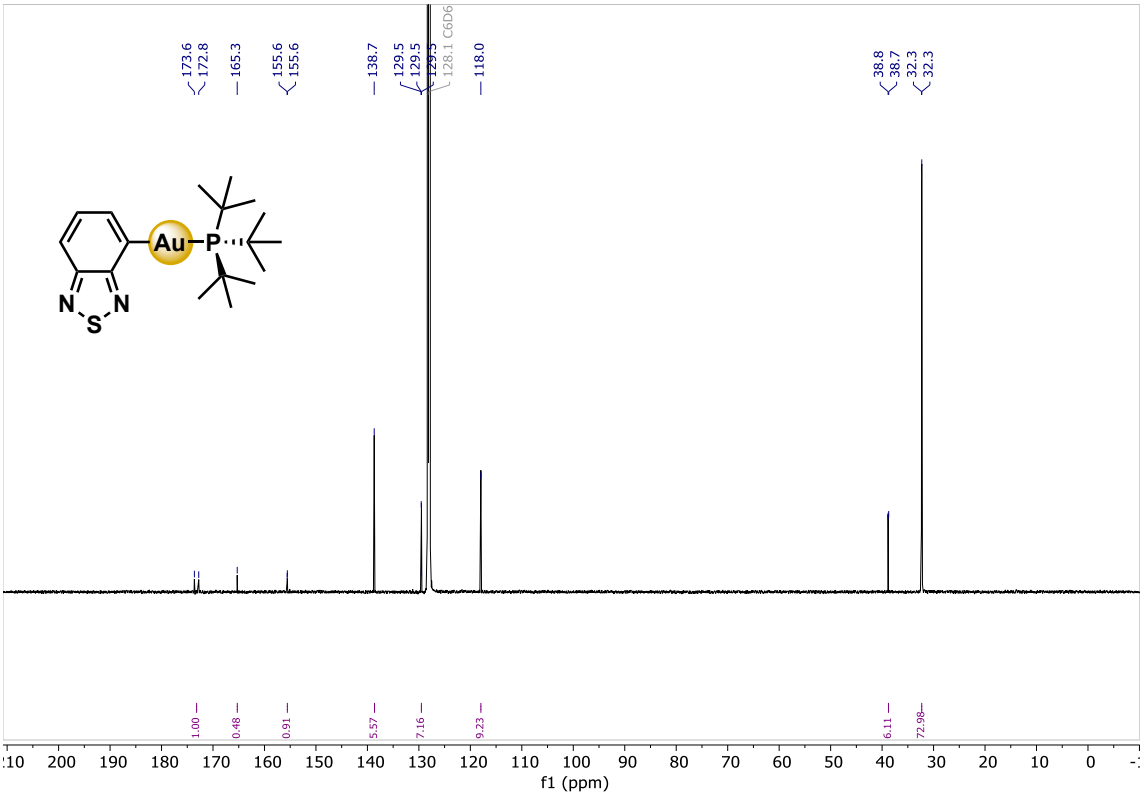

$^{31}$P NMR (162 MHz, $C_6D_6$) for compound **3b**.

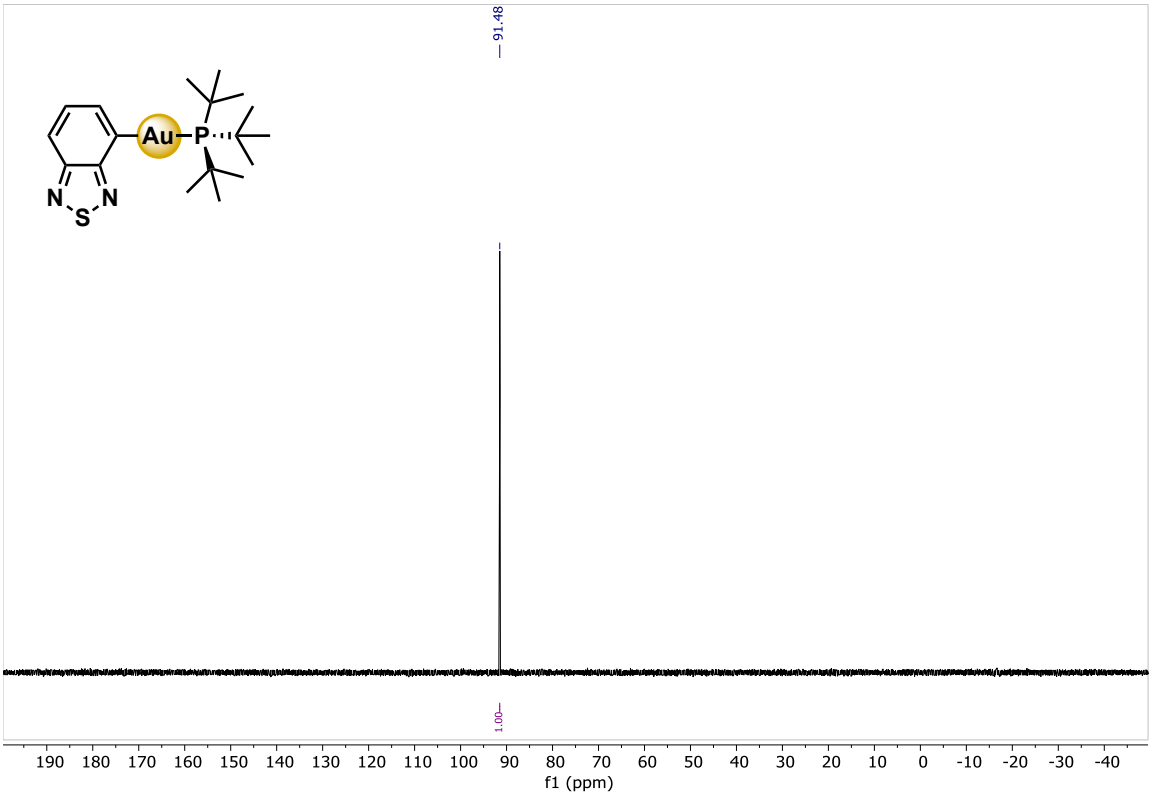


$^{1}$H NMR (400 MHz, $C_6D_6$) for compound **3c**.

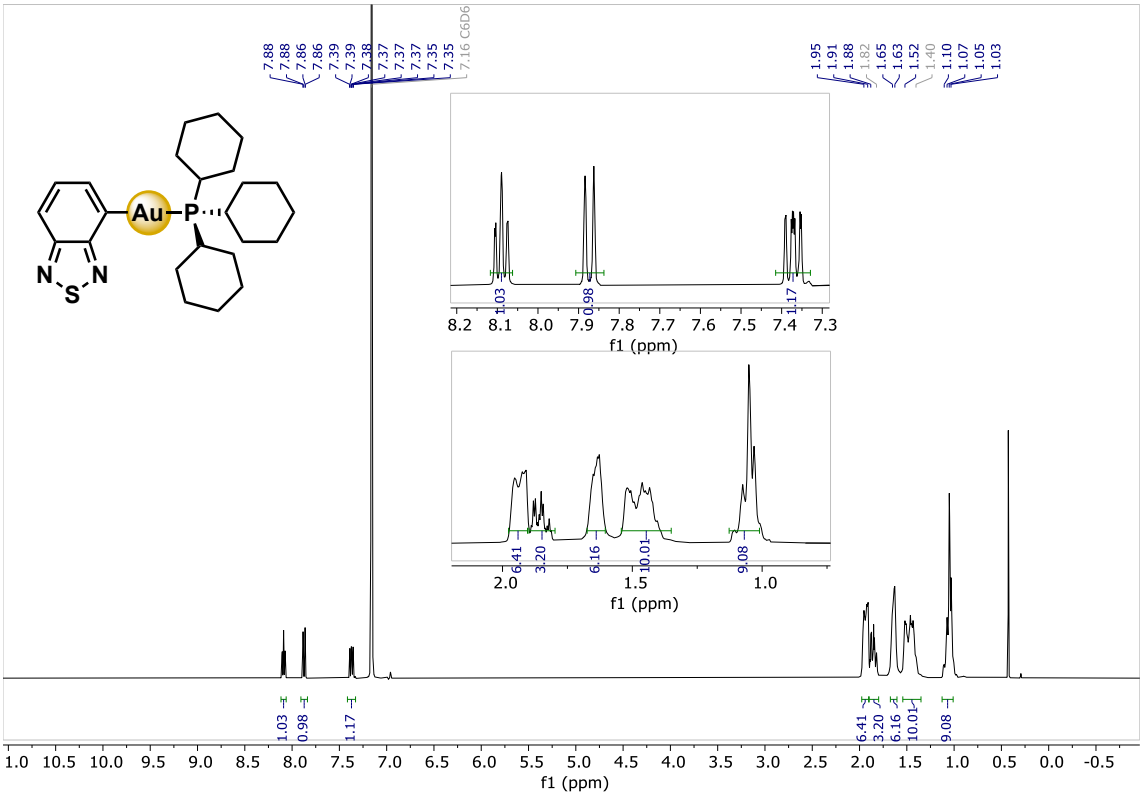

$^{13}$C NMR (101 MHz, $C_6D_6$) for compound **3c**.

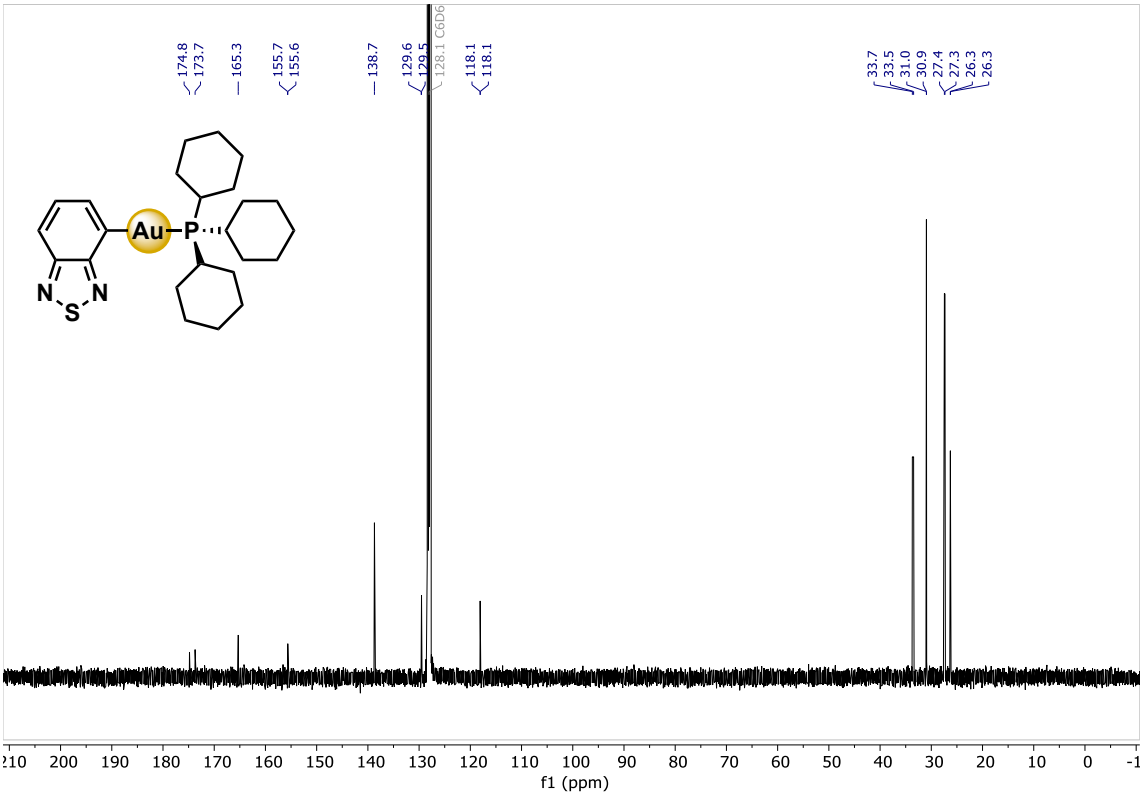


$^{31}$P NMR (162 MHz, $C_6D_6$) for compound **3c**.

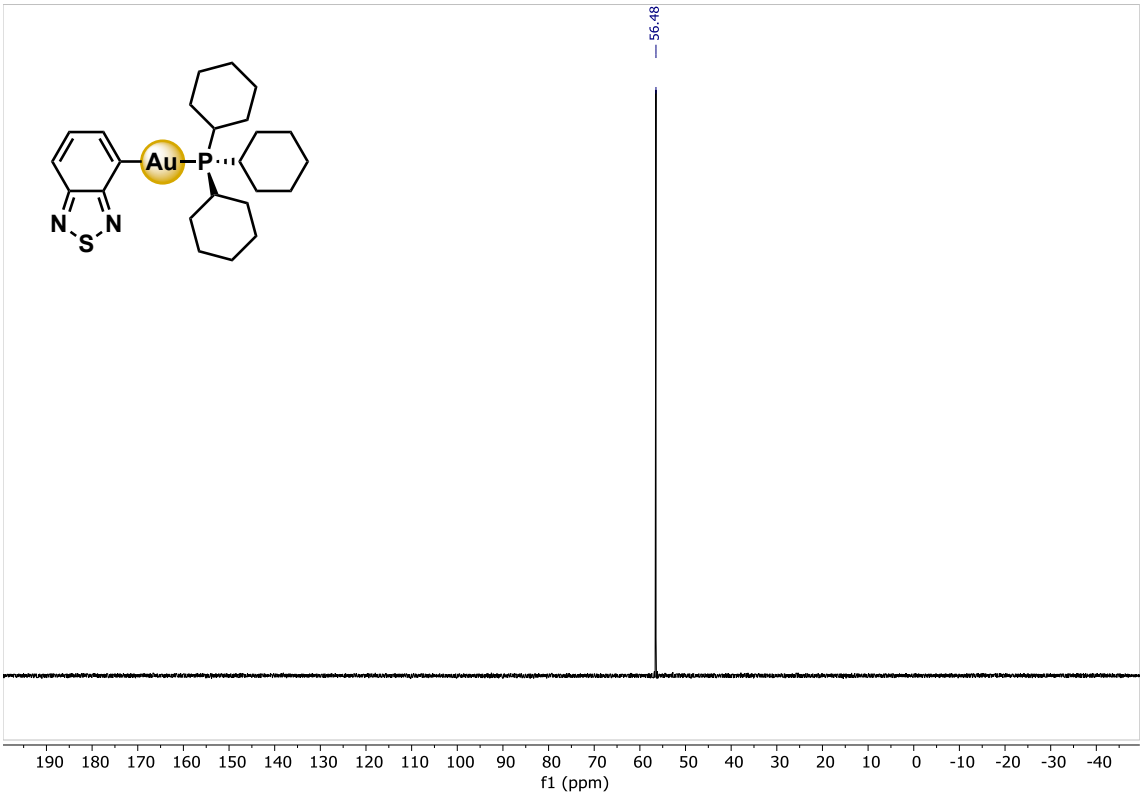

$^{1}$H NMR (400 MHz, $C_6D_6$) for compound **3d**.

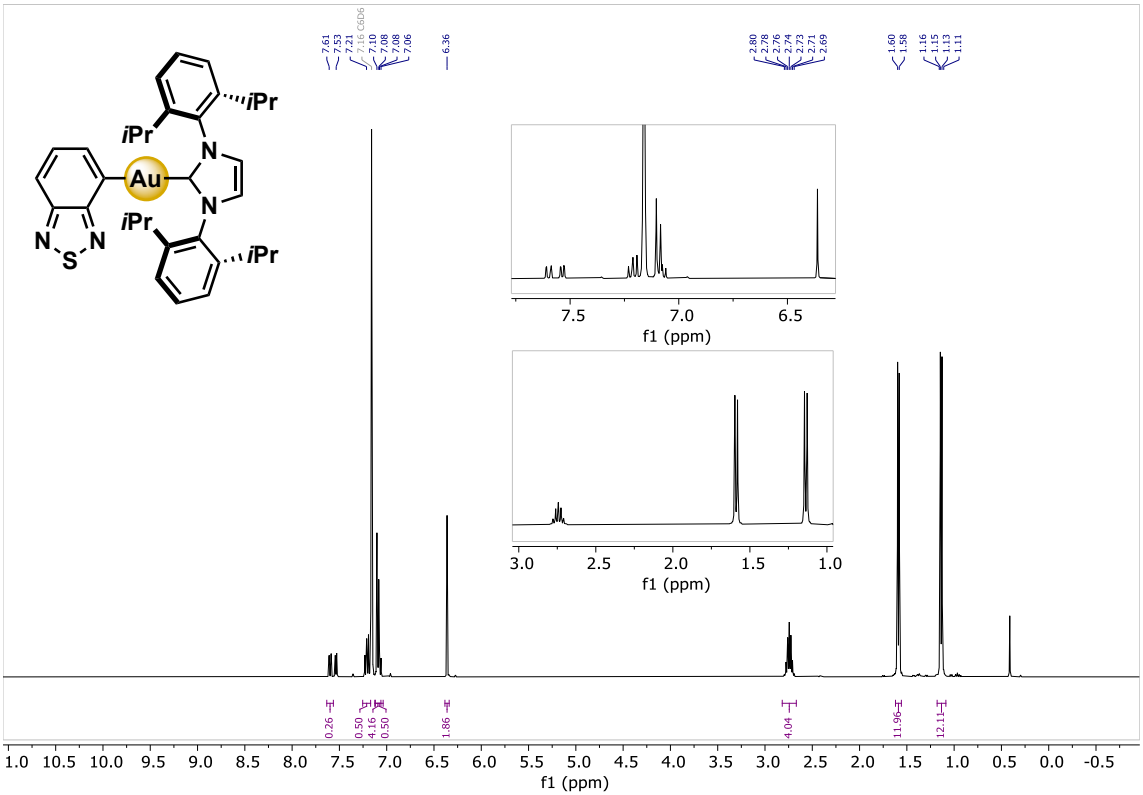


$^{13}$C NMR (101 MHz, $C_6D_6$) for compound **3d**.

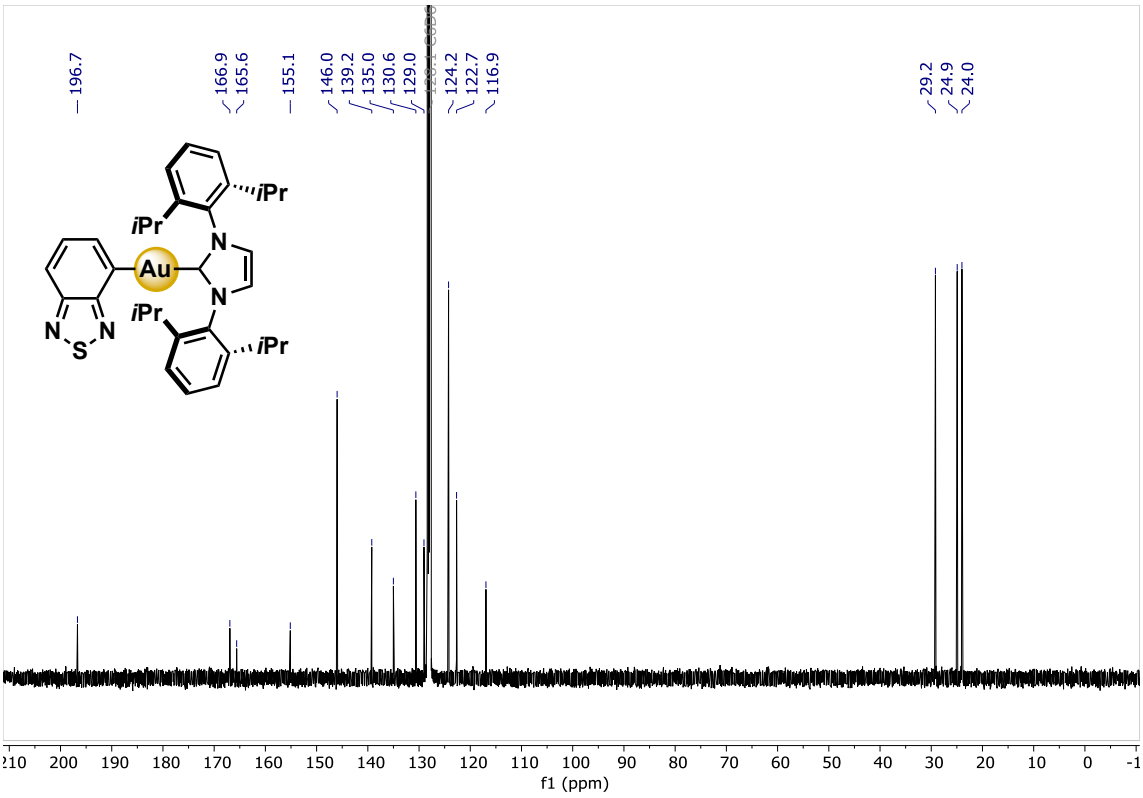

$^{1}$H NMR (400 MHz, $C_6D_6$) for compound **3e**.

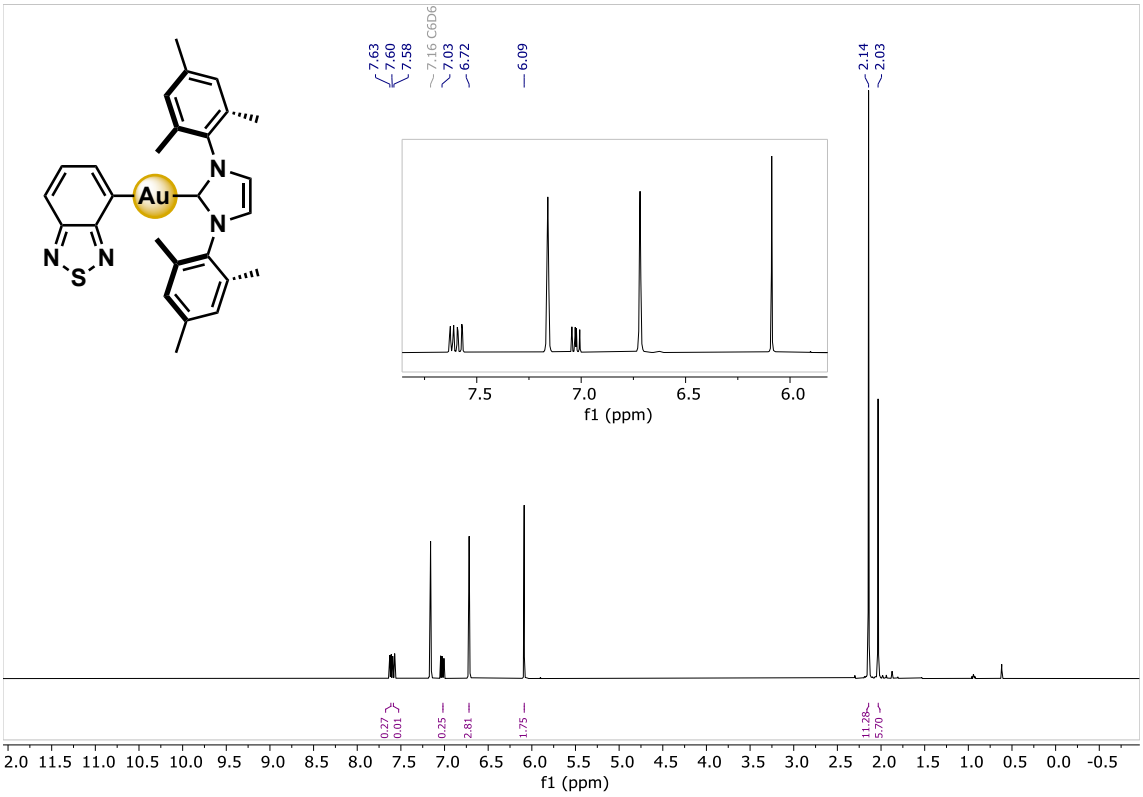


$^{13}$C NMR (101 MHz, $C_6D_6$) for compound **3e**.

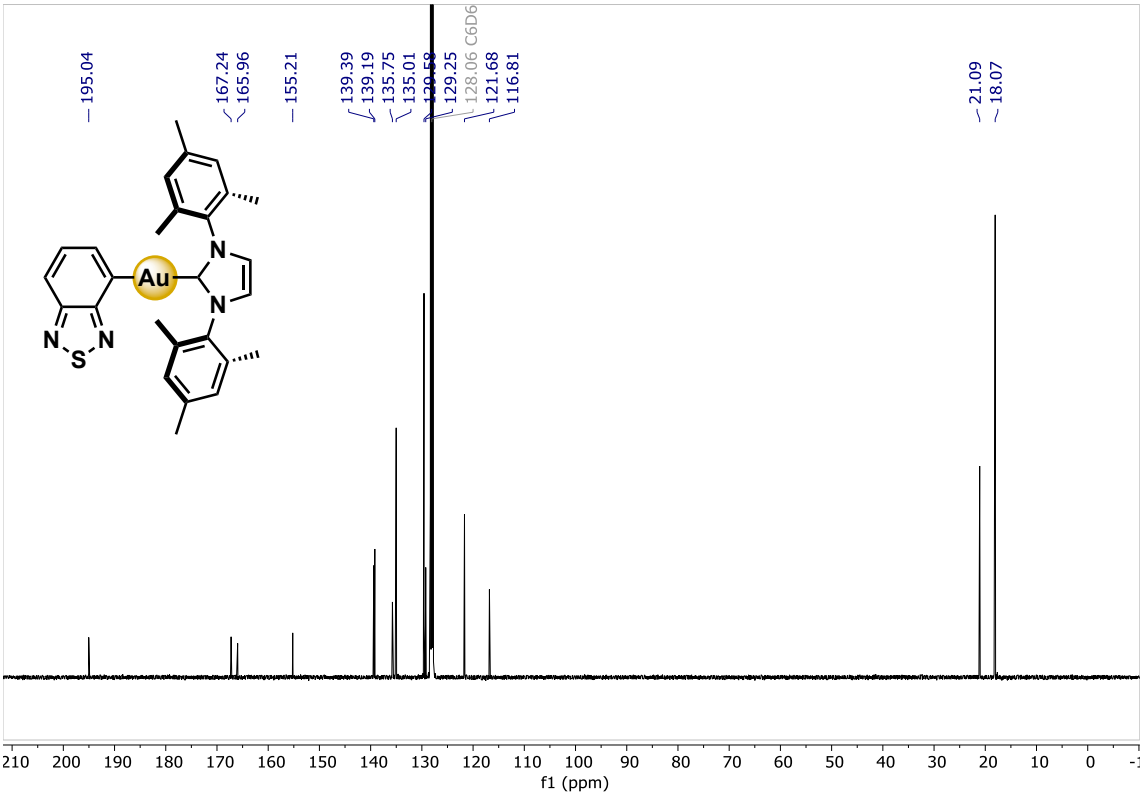

## References


1. H. Ishida, S. Tobita, Y. Hasegawa, R. Katoh and K. Nozaki, *Coord. Chem. Rev.*, 2010, **254**, 2449-2458.
2. *Journal*.
3. C. Adamo and V. Barone, *The Journal of Chemical Physics*, 1999, **110**, 6158-6170.
4. M. Cossi, G. Scalmani, N. Rega and V. Barone, *The Journal of Chemical Physics*, 2002, **117**, 43-54.
5. G. A. Petersson and M. A. Al-Laham, *The Journal of Chemical Physics*, 1991, **94**, 6081-6090.
6. M. M. Francl, W. J. Pietro, W. J. Hehre, J. S. Binkley, M. S. Gordon, D. J. DeFrees and J. A. Pople, *The Journal of Chemical Physics*, 1982, **77**, 3654-3665.
7. P. C. Hariharan and J. A. Pople, *Theoretica Chimica Acta*, 1973, **28**, 213-222.
8. D. Andrae, U. Häußermann, M. Dolg, H. Stoll and H. Preuß, *Theoretica chimica acta*, 1990, **77**, 123-141.
9. J. M. L. Martin and A. Sundermann, *The Journal of Chemical Physics*, 2001, **114**, 3408-3420.
10. K. T. Chan, G. S. M. Tong, W.-P. To, C. Yang, L. Du, D. L. Phillips and C.-M. Che, *Chem. Sci.*, 2017, **8**, 2352-2364.
11. G. S. Ming Tong, K. T. Chan, X. Chang and C.-M. Che, *Chemical Science*, 2015, **6**, 3026-3037.
12. I. Noviandri, K. N. Brown, D. S. Fleming, P. T. Gulyas, P. A. Lay, A. F. Masters and L. Phillips, *J. Phys. Chem. B*, 1999, **103**, 6713-6722.